Molecular Features Underlying Shp1/Shp2 Discrimination by Immune Checkpoint Receptors

Xiaozheng Xu[1,2], Takeya Masubuchi[1,2], Yunlong Zhao[1], & Enfu Hui[1,3]*

[1]Section of Cell & Developmental Biology, Division of Biological Sciences, University of California, San Diego, La Jolla, CA 92093-0347, USA

[2]These authors contribute equally

[3]Lead Contact

*Correspondence: enfuhui@ucsd.edu

Abstract

Numerous inhibitory immunoreceptors operate by recruiting phosphatase effectors Shp1 and Shp2 through conserved motifs ITIM and ITSM. Despite the similarity, these receptors exhibit distinct effector binding specificities, as exemplified by PD-1 and BTLA, which preferentially recruit Shp2 and Shp1 respectively. The molecular basis of Shp1/Shp2 discrimination is unclear. Here, we provide evidence that optimal PD-1 and BTLA binding to both Shp1 and Shp2 occurs via a bivalent, parallel mode that involves both SH2 domains of Shp1/Shp2. Moreover, PD-1 mainly uses its ITSM to discriminate Shp2 from Shp1 via their C-terminal SH2 domains. Supportive of this model, swapping the Shp1-cSH2 with Shp2-cSH2 enabled PD-1:Shp1 association in T cells. In contrast, BTLA primarily utilizes its ITIM to discriminate Shp1 from Shp2 via their N-terminal SH2 domains. Substitution of glycine at pY+1 position of the PD-1-ITIM with alanine, a residue conserved in several Shp1-recruiting receptors, was sufficient to induce PD-1:Shp1 interaction in T cells. Finally, mutagenesis screening shows that Shp1 recruitment exhibits a bell-shaped dependence on the side chain volume of the pY+1 residue of ITIM. Collectively, we provide a molecular interpretation of the Shp1/Shp2-binding specificities of PD-1 and BTLA, with general implications for the mechanism of effector discrimination by inhibitory receptors.

Keywords: PD-1, BTLA, Shp1, Shp2, ITIM, ITSM

25 **Main**

26 Signal transduction critically depends on phosphorylation that occurs both on cell surface receptors and
27 on their downstream effector molecules. Many signal-transducing proteins contain Src-Homology-2
28 (SH2) domains, a structural fold that binds to phosphotyrosine (pY) motifs[1,2]. Thus, tyrosine
29 phosphorylation can induce intermolecular interactions, when pY and SH2 exist in different proteins, or
30 intramolecular interactions, when pY and SH2 exist in the same protein. As such, tyrosine
31 phosphorylation acts as a switch for both protein-protein interactions and protein conformational
32 changes that dictate their functional activities.

33 In cells, two sets of enzymes reciprocally control the level of tyrosine phosphorylation: protein tyrosine
34 kinases (PTKs) which catalyze the phosphorylation of tyrosine residues, and protein tyrosine
35 phosphatases (PTPases) that catalyze the removal of phosphate groups from pY residues[3-6]. As a
36 prominent example, the T cell antigen receptor (TCR) complex and the costimulatory receptor CD28
37 both contain phosphorylatable tyrosines in their intracellular domains (ICDs). Phosphorylation of TCR
38 and CD28, catalyzed by the membrane-targeted PTK Lck[7-9], creates docking sites for SH2-containing,
39 cytoplasmic kinases and adaptor proteins that relay and amplify the receptor signal through well-
40 orchestrated phosphorylation cascades[10,11].

41 The phosphorylation-dependent TCR and CD28 signaling is opposed by inhibitory receptors such as
42 PD-1 and BTLA. These receptors recruit cytoplasmic PTPases[12-15] upon ligation to their respective
43 ligands, PD-L1/2[16-18] and HVEM[19-21], to dephosphorylate TCR and CD28 signaling components[22-24].
44 Both PD-1 and BTLA contain a single ITIM (immunoreceptor tyrosine-based inhibition motif;
45 S/I/V/LxYxxI/V/L) and a single ITSM (immunoreceptor tyrosine-based switch motif; TxYxxV/I),
46 conserved motifs found in many immunoreceptors[25-28]. Upon tyrosine phosphorylation, ITIM and ITSM
47 serve as docking sites for tandem SH2 domains (tSH2) contained in Shp1 and Shp2, structurally
48 similar, and yet functionally distinct cytoplasmic PTPases[29]. The PTPase domain of Shp1, but not that

49 of Shp2, was able to dephosphorylate Zap70 and Syk[30]. Moreover, Shp1-recruiting receptors more
50 potently suppress TCR and CD28 phosphorylation than do Shp2-recruiting receptors[24].

51 Despite the large number of ITIM/ITSM-containing receptors in the human genome, little is known
52 regarding their molecular mechanisms. There is sparse information about their specificities for Shp1 or
53 Shp2. Whether they signal through Shp1, Shp2, or both, and to what extent they prefer one over the
54 other, have not been well established. Indeed, growing evidence suggests that ITIM/ITSM-containing
55 receptors exhibit distinct specificities for Shp1 and Shp2 recruitment. PD-1 strongly recruits Shp2, but
56 not Shp1, in both T cells and B cells[14,23]. In contrast, BTLA prefers Shp1 over Shp2[24,31,32]. The
57 mechanism underlying the distinct PTPase-binding specificities of PD-1 and BTLA remains obscure.
58 This issue has been confounded by the multiple possible binding modes between a dual-tyrosine
59 receptor and a dual-SH2 protein, and the reported abilities of the Shp1/Shp2 to dephosphorylate their
60 docking sites within the receptor[22,23,33].

61 In this study, we dissected the molecular mechanisms by which PD-1 and BTLA discriminate between
62 Shp1 and Shp2. We measured the affinities of all potential pY:SH2 interactions involved in PD-1 and
63 BTLA recruitment of Shp1 and Shp2 using surface plasmon resonance (SPR), and identified the
64 optimal binding geometries of both Shp1 and Shp2. We then measured the recruitment of Shp1 and
65 Shp2 to PD-1 microclusters in intact T cells, using both wild-type (WT) and domain-swapped mutants.
66 These experiments have allowed us to identify key molecular features in PD-1 and BTLA that lead to
67 their specificity dichotomy. Our finding has implications to the specificities of the rapidly growing list of
68 immune checkpoint receptors.

69

70 **Results**

71 **PD-1 recruits Shp2, but not Shp1, whereas BTLA prefers to recruit Shp1**

72 Previous studies suggest that tyrosine-phosphorylated PD-1 recruits Shp2, but not Shp1, to suppress T
73 cell activation[23,34]. To begin investigating the molecular basis of this specificity, we utilized an antigen
74 presenting cell (APC) – T cell co-culture assay incorporating the PD-L1:PD-1 pathway. In this assay,
75 PD-1-mGFP transduced Jurkat T cells were stimulated with superantigen (SEE)-loaded, PD-L1
76 transduced Raji B cells (APCs). After lysing the cell conjugates at desired time points, we
77 immunoprecipitated (IP) PD-1-mGFP from the cell lysates and probed pY and co-precipitated Shp1 or
78 Shp2 using immunoblots (IB). PD-1 became tyrosine phosphorylated, and recruited Shp2 but not Shp1
79 in a time-dependent fashion (**Fig. 1a**), consistent with recent studies[23,24]. By contrast, in a parallel co-
80 culture system containing HVEM transduced Raji cells and BTLA-mGFP transduced Jurkat cells, BTLA
81 recruited both Shp1 and Shp2, with a clear preference for Shp1 (**Fig. 1b**), consistent with recent
82 studies[24,31,32].

83 **Both ITIM and ITSM contribute to the ability of PD-1 to recruit Shp2**

84 We next attempted to clarify the relative contributions of ITIM and ITSM in mediating Shp2 recruitment,
85 by examining how mutations of these motifs affect Shp2 binding and PD-1 function. We generated
86 Jurkat cells expressing similar levels of mGFP-tagged PD-1^{WT}, PD-1^{FY}, in which the ITIM Y223 was
87 mutated to phenylalanine, PD-1^{YF}, in which the ITSM Y248 was mutated to phenylalanine, or PD-1^{FF}, in
88 which both tyrosines were mutated (**Extended Data Fig. 1a**). Upon stimulation with PD-L1-transduced
89 Raji cells, we detected Shp2 but not Shp1 in the PD-1^{WT} IP (GFP IP), and as expected, Shp2 was
90 undetectable in PD-1^{FF} IP samples. The ITSM mutant PD-1^{YF} also failed to recruit Shp2, whereas the
91 ITIM mutant PD-1^{FY} recruited Shp2, but significantly less than PD-1^{WT} (**Fig. 2a**). We confirmed these
92 observations by visualizing PD-1:Shp2 interaction in intact T cells. We plated the foregoing Jurkat cells
93 on a supported lipid bilayer (SLB) containing anti-CD3ε (for TCR stimulation) and recombinant PD-L1
94 ectodomain (PD-L1^{ECD}, for PD-1 stimulation). Total internal reflection microscopy (TIRF-M) in the GFP
95 channel revealed PD-1 microclusters in all four cell-types (**Fig. 2b**). Immunostaining of Shp2 showed
96 strong enrichment of Shp2 to PD-1^{WT} microclusters. Shp2 recruitment was slightly weaker for PD-1^{FY},
97 but statistically significant ($p=0.0306$), and Shp2 recruitment was almost completely abrogated in PD-

98 1^{YF}, similar to the negative control PD-1^{FF} (**Fig. 2b**). These data are in general agreement with previous
99 reports that ITSM is the dominant docking site for Shp2[12,14,23,35,36]. However, our result showed that PD-
100 1^{WT} recruited more Shp2 than did PD-1^{FY}, suggesting that optimal Shp2 recruitment does require ITIM.
101 The more obvious defect of PD-1^{FY} in the co-IP assays might be due to the disruption of weak
102 interactions by the non-equilibrium wash steps.

103 **PD-1-ITSM strongly prefers Shp2-cSH2 over Shp1-cSH2**

104 We next investigated the molecular mechanism by which PD-1 recruits Shp2 but not Shp1 in T cells.
105 Shp1 and Shp2 both contain two SH2 domains in tandem, the N-terminal SH2 (nSH2) and the C-
106 terminal SH2 (cSH2). Our co-IP data indicated that Shp2 interacts with PD-1 in a bivalent fashion
107 involving both SH2 domains. The bivalent interaction can potentially occur either in a parallel fashion in
108 which nSH2 binds to ITIM and cSH2 binds to ITSM, or in an antiparallel fashion in which nSH2 and
109 cSH2 bind to ITSM and ITIM respectively. To determine the most favorable binding orientation, we next
110 measured the affinities for all the possible pY:SH2 interactions implicated in PD-1:Shp1 and PD-1:Shp2
111 interactions. We purified pre-phosphorylated ICDs of PD-1 mutants that contained only one tyrosine
112 within either ITIM (PD-1^{YF}) or ITSM (PD-1^{FY}). We then used SPR to measure their binding affinities to
113 purified Shp1-nSH2, Shp1-cSH2, Shp2-nSH2, and Shp2-cSH2 (**Fig. 3a**), and summarized the
114 dissociation constants (K_d) in **Supplementary Table 1**.

115 To summarize the SPR data, we diagramed all the detectable SH2:pY interactions in the context of
116 tandem SH2 and PD-1^{WT}, with relative affinities depicted by arrow thickness. PD-1-ITSM is a better
117 docking site than is PD-1-ITIM for each of the four SH2 tested (**Fig. 3b**). A careful inspection of the data
118 also revealed specific information, as detailed below.

119 For PD-1:Shp2 interactions, Shp2-nSH2 weakly preferred PD-1-ITSM (K_d = 0.14 μM) over PD-1-ITIM
120 (K_d = 0.38 μM), and Shp2-cSH2 strongly preferred PD-1-ITSM (K_d = 0.10 μM) over PD-1-ITIM (K_d = 1.4
121 μM) (**Fig. 3a**,**b**; **Supplementary Table 1**). Thus, the parallel mode PD-1:Shp2 complex would be more

energetically favorable than the antiparallel mode (**Fig. 3c**, right; **Supplementary Tables 2** and **3**), consistent with a recent report[37].

For PD-1:Shp1 interactions, Shp1-nSH2 preferred PD-1-ITSM (K_d = 0.083 μM) over PD-1-ITIM (K_d = 0.27 μM). Interestingly, Shp1-cSH2 appeared to be defective in PD-1 binding, exhibiting a rather weak affinity to PD-1-ITSM (K_d = 1.7 μM), and no detectable binding to PD-1-ITIM (**Fig. 3a**,**b**; **Supplementary Table 1**). The inability of Shp1-cSH2 to bind PD-1-ITIM ruled out the anti-parallel mode of PD-1:Shp1 interactions, but indicated the possibility of a monovalent mode in which Shp1-nSH2 interacts with PD-1-ITSM (**Fig. 3c**, left). However, free energy calculations suggested that the parallel mode, which involves two SH2, is energetically favorable over the monovalent mode (**Supplementary Table 2** and **3**).

To further examine the dominant mode of PD-1:Shp1 interactions, we employed a single molecule assay to determine whether PD-1:Shp1 interactions require only ITSM, as would be expected for the monovalent mode, or both ITIM and ITSM, as would be expected for the bivalent parallel mode. We sparsely attached monomeric, fluorescently-labeled, pre-phosphorylated and biotinylated PD-1^{WT}, PD-1^{FY}, or PD-1^{YF} (**Extended Data Fig. 2a**,**b**) to a biotin polyethylene glycol (PEG)-coated coverslip via streptavidin. TIRF-M resolved individual PD-1 monomers as discrete spots, which underwent photobleaching in single steps (**Extended Data Fig. 2c**,**d**). After the addition of JF646-labeled tSH2 of either Shp1 or Shp2, we visualized PD-1:tSH2 interaction at the coverslip (**Extended Data Fig. 2e**, left). Recruitment of Shp2-tSH2 to PD-1 led to the appearance of JF646 signal that colocalized with PD-1 molecules (**Extended Data Fig. 2e**, upper right). Each Shp2-tSH2 spot typically persisted for several seconds, then disappeared due to dissociation from PD-1, leading to a step-like time course (**Extended Data Fig. 2e**, lower right). As expected, Shp1-tSH2 displayed a lower degree of PD-1 occupancy (**Extended Data Fig. 2f**). Moreover, mutation of either ITIM (PD-1^{FY}) or ITSM (PD-1^{YF}) strongly reduced the PD-1 occupancy for both Shp1-tSH2 and Shp2-tSH2, as compared to the WT control (PD-1^{WT}) (**Extended Data Fig. 2f**), further supporting that both Shp1-tSH2 and Shp2-tSH2 binds to PD-1^{WT} in a bivalent fashion involving both ITIM and ITSM.

148 Collectively, data presented in this section demonstrated that both Shp1 and Shp2 interact with PD-1
149 primarily via the bivalent parallel geometry. However, the PD-1:Shp1 interaction is much less stable
150 due to the very weak affinity between Shp1-cSH2 and PD-1-ITSM.

151

152 **Replacement of Shp1-cSH2 by Shp2-cSH2 is sufficient to induce PD-1:Shp1 association in T**
153 **cells**

154 The SPR data (**Fig. 3b**; **Supplementary Table 1**) indicated that the Shp1-cSH2 barely interacts with
155 PD-1-ITSM, whereas Shp2-cSH2 displayed a 17-fold higher affinity to the ITSM of PD-1. Thus, we next
156 determined if swapping the cSH2 of Shp1 with that of Shp2 could induce PD-1:Shp1 binding in T cells.
157 We sought to image the recruitment of domain-swapped chimeric mutants of Shp1 to PD-1
158 microclusters. To avoid competition from endogenous Shp1 and Shp2, we generated Shp1/Shp2
159 double knockout (DKO) Jurkat cells, and co-transduced PD-1-mGFP with mCherry-tagged $Shp1^{WT}$ or
160 Shp1 mutant with one or both of its SH2 domains replaced by those of Shp2 (**Fig. 4a**). Having
161 confirmed that these cells expressed similar levels of PD-1-mGFP and mCherry-tagged Shp1 variants
162 (**Extended Data Fig. 1b**), we stimulated each type of Jurkat cells with a SLB containing anti-CD3ε and
163 $PD\text{-}L1^{ECD}$.

164 TIRF-M showed that upon cell-bilayer contact, PD-1 formed microclusters that recruited little to no
165 $Shp1^{WT}$, as manifested by nearly undetectable mCherry signal in the GFP foci (**Fig. 4b**, top row),
166 consistent with previous reports[23,24]. Swapping the nSH2 of Shp1 with that of Shp2 ($Shp1^{Shp2\text{-}nSH2}$)
167 increased the mCherry signal in PD-1 microclusters, but only to a minor degree (**Fig. 4b**, second row).
168 In contrast, swapping the cSH2 of Shp1 with that of Shp2 ($Shp1^{Shp2\text{-}cSH2}$) led to a marked increase in
169 mCherry signal in the PD-1 microclusters (**Fig. 4b**, third row), to a comparable extent as $Shp1^{Shp2\text{-}tSH2}$,
170 in which both SH2 of Shp1 were replaced with those of Shp2 (**Fig. 4b**, bottom row).

171 We confirmed the TIRF results using a co-IP assay. After stimulation of the foregoing Jurkat cells (**Fig.**
172 **4b**) with PD-L1-transduced Raji cells, we pulled down PD-1-mGFP and examined the co-precipitated
173 Shp1 variants using IB. We detected no signal of $Shp1^{WT}$, weak signal of $Shp1^{Shp2\text{-}nSH2}$, and strong
174 signal of $Shp1^{Shp2\text{-}cSH2}$ and $Shp1^{Shp2\text{-}tSH2}$ (**Fig. 4c**, GFP IP, Shp1 IB). Notably, PD-1 phosphorylation was
175 inversely correlated with the recruitment of the Shp1 variants (**Fig. 4c**, GFP IP, pY IB), supporting the
176 notion that PD-1 is also a substrate for its bound PTPases[22,23,33].

177 Collectively, data reported in this section demonstrated that cSH2 is the major determinant underlying
178 PD-1's strong preference for Shp2 over Shp1.

179 **ITIM and ITSM are both required for BTLA to recruit Shp1/Shp2**

180 Having established deficient ITSM:cSH2 interactions as the primary basis for the reduced stability of
181 PD-1:Shp1 binding, we next turned our attention to receptors that normally recruit Shp1 in T cells, such
182 as BTLA (**Fig. 1b**) to gain further insights into the mechanisms of effector PTPase discrimination by
183 ITSM/ITIM-bearing receptors[13,24,31]. We wished to determine the structural features in BTLA that
184 enabled its Shp1 recruitment in T cells.

185 The ICD of human BTLA harbors four phosphorylatable tyrosines (Y226, Y243, Y257 and Y282), in
186 which Y257 and Y282 are embedded in ITIM and ITSM respectively. We first asked which tyrosine of
187 BTLA are required for Shp1 and Shp2 recruitment. Analogous to PD-1 assays (**Fig. 2a**), we established
188 Jurkat cell lines expressing either WT or mutant BTLA in which one of the four phosphorylatable
189 tyrosine was replaced by phenylalanine (**Fig. 5a**). We then stimulated these cell lines, in parallel, with
190 HVEM-expressing Raji B cells. Co-IP experiments showed that the mutation of either or both of the
191 non-ITIM/ITSM phosphorylatable tyrosines (Y226F: $BTLA^{FYYY}$; Y243F: $BTLA^{YFYY}$; Y226F & Y243F:
192 $BTLA^{FFYY}$) had little to no effect on the abilities of BTLA to recruit Shp1/Shp2 (**Fig. 5b** and **Extended**
193 **Data Fig. 3**), demonstrating that these two tyrosines are dispensable for BTLA-mediated recruitment of
194 Shp1/Shp2. In contrast, mutation of either ITIM tyrosine (Y257F: $BTLA^{YYFY}$) or ITSM tyrosine (Y282F:

195 BTLA^{YYYF}) abolished the binding of both Shp1 and Shp2 (**Fig. 5b**), consistent with previous studies[13].
196 Thus, ITIM and ITSM are both necessary for Shp1 and Shp2 recruitment by BTLA. These data also
197 suggest that both SH2 domains of Shp1 and Shp2 are required for their recruitment to BTLA. The more
198 stringent requirement of both ITIM and ITSM of BTLA indicates that its ITIM and ITSM play more
199 balanced roles in mediating Shp1/Shp2 recruitment than those of PD-1.

200 **Shp1 and Shp2 both interact with BTLA via the bivalent parallel mode**

201 We next wished to determine the most favorable binding geometries for BTLA:Shp1 interactions and
202 BTLA:Shp2 interactions. Analogous to SPR assays with PD-1 (**Fig. 3**), we measured the affinities of
203 individual pY:SH2 interaction implicated in BTLA:Shp1/Shp2 interactions, using sensor chips coated
204 with pre-phosphorylated BTLA triple-tyrosine-mutant FFYF (BTLA-ITIM), which contained a lone
205 tyrosine (Y257) in its ITIM, or pre-phosphorylated BTLA triple-tyrosine-mutant FFFY (BTLA-ITSM),
206 which contained a lone tyrosine (Y282) in its ITSM (**Fig. 6a**). These experiments revealed that for both
207 Shp1 and Shp2, their nSH2 and cSH2 prefer BTLA-ITIM and BTLA-ITSM, respectively (**Fig. 6a**,**b**;
208 **Supplementary Table 1**). Thus, we concluded that the most favorable BTLA:Shp1 and BTLA:Shp2
209 interactions both occur in a parallel mode (**Fig. 6c**), similar to PD-1:Shp1 and PD-1:Shp2 interactions.

210 **BTLA-ITIM is a high-affinity docking site for Shp1-nSH2**

211 On a closer inspection of the SPR data, we found that the relative contribution of ITIM and ITSM in
212 BTLA is opposite to that in PD-1. While the ITSM is the major SH2 docking site in PD-1, the ITIM
213 appeared to be the major SH2 docking site in BTLA. This is particularly striking in the case of
214 BTLA:Shp1 interaction: Shp1-nSH2 exhibited an impressive affinity to BTLA-ITIM (K_d = 0.064 μM), 13-
215 fold higher than the affinity between Shp1-cSH2 and BTLA-ITSM (K_d = 0.86 μM) (**Fig. 6a** and
216 **Supplementary Table 1**).

217 Notably, the affinity of Shp1-nSH2 to BTLA-ITIM (K_d = 0.064 μM) was also four-fold higher than its
218 affinity to PD-1-ITIM (K_d = 0.27 μM) (**Fig. 6a** and **Supplementary Table 1**). Thus, even though both
219 BTLA-ITSM and PD-1-ITSM are poor docking sites for Shp1-cSH2, BTLA-ITIM is a much better
220 docking site for Shp1-nSH2 than is PD-1-ITIM. Conceivably, the strong BTLA-ITIM:Shp1-nSH2
221 interaction may compensate the weak BTLA-ITSM:Shp1-cSH2 interaction, leading to an overall stable
222 BTLA:Shp1 association in T cells.

223 **Swapping PD-1-ITIM with BTLA-ITIM induced PD-1:Shp1 interaction in T cells**

224 The foregoing data support a hypothesis that the stability of ITIM:SH2 interactions is vital for
225 ITIM/ITSM-bearing receptors to recruit Shp1. To test this experimentally, we assayed whether replacing
226 the "low affinity" ITIM of PD-1 with the 'high affinity' ITIM of BTLA could induce PD-1:Shp1 interaction.
227 We transduced Jurkat cells with either mGFP-tagged PD-1^{WT} or PD-1$^{BTLA\text{-}ITIM}$, in which we replaced PD-
228 1-ITIM (VDYGEL) with BTLA-ITIM (IVYASL) (**Fig. 7a** and **Extended Data Fig. 1c**). Following
229 stimulation of both types of Jurkat cells using PD-L1-expressing Raji B cells, co-IP assays revealed that
230 PD-1$^{BTLA\text{-}ITIM}$, but not PD-1^{WT} recruited Shp1 (**Fig. 7b**). We confirmed this finding using Shp2 KO Jurkat
231 cells, which allowed us to examine PD-1:Shp1 interaction without potential competition from Shp2 (**Fig.**
232 **7a**,**b**). We further verified these findings in intact cells using TIRF-M. In the cell-SLB assays, we
233 observed microclusters of both PD-1^{WT} and PD-1$^{BTLA\text{-}ITIM}$, and confirmed that the PD-1$^{BTLA\text{-}ITIM}$
234 microclusters recruited significantly more Shp1 than did the PD-1^{WT} microclusters (**Fig. 7c**). Finally, in a
235 reciprocal set of experiments, we found that replacement of the BTLA-ITIM with the PD-1-ITIM
236 markedly decreased the Shp1 recruitment to BTLA, in both WT Jurkat and Shp2 KO Jurkat cells
237 (**Extended Data Fig. 4**). Together, data presented in this section demonstrated that Shp1 primarily
238 discriminates BTLA from PD-1 based on their ITIMs.

239 **Replacement of the pY+1 glycine in PD-1-ITIM with alanine was sufficient to induce PD-1:Shp1**
240 **association in T cells**

241 We noted that the BTLA-ITIM (IVYASL) differ from PD-1-ITIM (VDYGEL) at four residues flanking pY:
242 V221, D222, G224 and E225 in PD-1-ITIM are replaced by I, V, A and S respectively in BTLA-ITIM
243 (**Fig. 8a**). We wished to determine which replacement contributed the most in inducing Shp1 binding of
244 PD-1$^{BTLA\text{-}ITIM}$. We generated Shp2 KO Jurkat cells expressing comparable levels of PD-1^{V221I}, PD-1^{D222V},
245 PD-1^{G224A}, or PD-1^{E225S}, and each harbored a C-terminal mGFP (**Extended Data Fig. 1d**), and asked
246 which mutants were able to recruit Shp1. We also used cells expressing PD-1^{WT}-mGFP and cells
247 expressing PD-1$^{BTLA\text{-}ITIM}$-mGFP as controls. Upon stimulation with PD-L1-transduced Raji cells, we
248 IP'ed PD-1-mGFP and blotted for Shp1. As expected, Shp1 signal was evident in the precipitates of
249 PD-1$^{BTLA\text{-}ITIM}$ but not in PD-1^{WT}. Notably, PD-1^{G224A} also recruited the most Shp1 among the single point
250 mutants, despite less than PD-1$^{BTLA\text{-}ITIM}$, the positive control (**Fig. 8b**).

251 We next validated these findings using TIRF imaging of SLB-stimulated T cells. We observed PD-1
252 microclusters for all six PD-1 variants. Consistent with **Fig. 7c**, microclusters of PD-1$^{BTLA\text{-}ITIM}$, but not
253 PD-1^{WT} recruited Shp1 (**Fig. 8c**, rows 1 and 2). Among the single point mutants, only PD-1^{G224A}
254 microclusters clearly recruited Shp1 (**Fig. 8c**, row 5), albeit less than did PD-1$^{BTLA\text{-}ITIM}$ microclusters
255 when Shp1 signal was normalized to the PD-1 signal (dot plot). In contrast, the other three single point
256 mutants (PD-1^{V221I}, PD-1^{D222V}, and PD-1^{E225S}) showed little to no Shp1 recruitment (**Fig. 8c**, rows 3, 4
257 and 6). These experiments suggested that the alanine residue at the pY+1 position of the ITIM motif
258 promotes Shp1 binding.

259 Indeed, sequence alignment revealed that alanine is conserved at pY+1 position of ITIM in several
260 inhibitory receptors (**Extended Data Fig. 5**), including Siglec-6, Siglec-9, CD300LF, VSTM4, and
261 SIRPα, most of which reportedly recruit Shp1[26,38-41]. As expected, swapping the PD-1-ITIM by the ITIM
262 of the foregoing inhibitory receptors (**Fig. 8d** and **Extended Data Fig. 1e**) significantly increased Shp1
263 recruitment to PD-1 immunoprecipitates and PD-1 microclusters, as compared to PD-1^{WT} (**Fig. 8e**,**f**).

264 **A medium-sized nonpolar residue at pY+1 position of the ITIM is required for Shp1 recruitment**

265 The ability of somewhat conservative mutation (G224A) to induce PD-1:Shp1 binding was unexpected,
266 however, given that alanine has a larger side chain than does glycine, we next sought to determine how
267 the side chain property of pY+1 position influences PD-1:Shp1 interaction. Therefore, we mutated the
268 glycine to a series of residues that differ in the size and polarity of their side chains. We established
269 Jurkat cell lines that express each of the PD-1 mutants fused to a GFP tag, at comparable levels
270 indicated by flow cytometry (**Extended Data Fig. 1f**). In the cell-SLB assay, we found that PD-1
271 mutants containing a medium-sized nonpolar residue at pY+1 position (G224A, G224V, G224L, G224I)
272 most strongly recruited Shp1 (**Fig. 9a**, rows 3-6), a bulky or rigid nonpolar residue at this position
273 (G224F, G224W, and G224P) decreased the Shp1 recruitment (**Fig. 9a**, rows 7-9). Indeed, plotting the
274 Shp1 recruitment against the side chain volume of the five nonpolar residues, excluding the rigid
275 proline, revealed a bell-shaped dependence that peaked at leucine and isoleucine (**Fig. 9b**). Finally, a
276 polar or charged residue at this position failed to induce Shp1 recruitment, as observed for G224S,
277 G224T, G224K and G224D mutants (**Fig. 9a**, rows 10-13). Taken together, these results revealed that
278 a medium-sized nonpolar residue at pY+1 position of the ITIM is required for Shp1 recruitment. It is
279 likely that Shp1-nSH2 contains a hydrophobic pocket that coordinates a medium-sized side chain of the
280 pY+1 residue of ITIM.

281 **Discussion**

282 Shp1 and Shp2 are key regulators of cell survival, proliferation, differentiation, and migration[29,42-45]. Co-
283 expressed in hematopoietic cells, they operate as central effectors for immune inhibitory receptors that
284 contain ITIM and ITSM. Dissecting the precise mechanism by which these receptors discriminate
285 between Shp1 and Shp2 is required to predict and understand their “checkpoint” functions. In the
286 present work, we combined biophysical, biochemical and cellular imaging approaches to investigate the
287 specificity dichotomy of PD-1 and BTLA. Our data have revealed distinct properties between the SH2
288 domains of Shp1 and Shp2, and between the ITIMs of these two checkpoint receptors. We also report
289 that the differential Shp1-binding activities of PD-1 and BTLA can be largely attributed to a single

290 (pY+1) residue of their ITIMs: our data show that the polarity and size of this residue gate Shp1
291 recruitment in T cells.

292 In human genome, at least 32 receptors contain two or more ITIMs or ITSMs in tandem. Conceivably,
293 the tandem pY motifs favor their bivalent interactions with tSH2 of Shp1 and Shp2. Mathematical
294 modeling predicts that bivalent binding, even contributed by two weak bonds, can produce stable
295 protein complexes due to the avidity effect and a reduction of off-rate of protein complexes[46]. In support
296 of this notion, an earlier study showed that mutation of either ITIM or ITSM of BTLA abolishes its
297 association with both Shp1 and Shp2[15], a result that we have confirmed in the present study (**Fig. 5b**).
298 The bivalent binding mode appears to be less strict in the case of PD-1, since its ITIM mutant retained
299 the ability to co-IP Shp2[12,14,23,35,36]. A recent study suggested that Shp2 may crosslink two PD-1
300 molecules at the ITSM[36], whereas other studies indicate that PD-1-ITIM contributes to Shp2 recruitment
301 and activation[23,35,37]. In our hands, ITIM mutant recruited significantly less Shp2 than PD-1^{WT} in co-IP,
302 microcluster enrichment and single molecule assays, supporting the involvement of ITIM, and the 1:1
303 bivalent mode as the dominant mode of PD-1:Shp2 interaction (**Fig. 2** and **Extended Data Fig. 2**). In
304 both BTLA and PD-1, the ITIM tyrosine and ITSM tyrosine are separated by 25 residues[27], and similar
305 spacing are found in numerous ITIM/ITSM-containing receptors (**Supplementary Table 4**). This
306 conserved distance may allow for simultaneous engagement of the ITIM and ITSM by the tSH2 of
307 Shp1/Shp2 in the 1:1 bivalent mode. The bivalent binding likely occurs in a sequential fashion, in which
308 the higher-affinity intermolecular contact precedes and converts the low affinity binding to a pseudo-
309 intramolecular event, as supported by mathematical modeling[47].

310 Our SPR data revealed certain promiscuities in the binding of their SH2 to ITIM and ITSM (**Figs. 3** and
311 **6**). Theoretically, Shp1 and Shp2 may bind to PD-1 and BTLA in either a parallel or an antiparallel
312 orientation. However, free energy calculations suggest parallel mode as the most stable form for both
313 PD-1 and BTLA (**Supplementary Table 2**), consistent with a recent study on PD-1:Shp2 interaction[37]
314 and an earlier study on PECAM1:Shp2 interaction[48]. To our knowledge, all ITIM/ITSM receptors with
315 the exception of SLAMF5 in human genome contain an ITIM N-terminal to ITSM (**Supplementary**

316 **Table 4**). This spatial arrangement might allow these receptors to bind Shp1 and Shp2 in the parallel
317 mode. The physiological significance of parallel binding is unclear, but it might increase the molecular
318 reach of the PTPase domain[49,50], or avoid potential steric clash with the plasma membrane.

319 Extensive genetic and biochemical evidence show that Shp1 and Shp2 differ in their physiological
320 functions. Shp2 reportedly acts as both a positive and negative regulator whereas Shp1 is primarily
321 known as a negative regulator in cell signaling[29,51]. The biochemical basis of their functional divergence
322 is unknown. The most striking difference between Shp1 and Shp2, based on the current study, are their
323 cSH2 domains: while Shp2-cSH2 binds to PD-1-ITSM with high affinity, Shp1-cSH2 exhibits weak to no
324 binding to PD-1-ITSM (**Fig. 3a**,**b**). This distinction account for the undetectable PD-1:Shp1 association
325 in T cells[23,24], supported by our domain-swapping experiments (**Fig. 4**). Thus, PD-1 prefers Shp2 over
326 Shp1 primarily based upon the stability of ITSM:cSH2 interaction. We speculate, in a more general
327 sense, that the differing cSH2 domains of Shp1 and Shp2 might enable their recruitment to distinct
328 signalosomes, leading to differing functional outcomes[29,51]. Indeed, Shp1-cSH2 and Shp2-cSH2 exhibit
329 51.9% homology in amino acid identities, and based on a recent nuclear magnetic resonance
330 structure[37], several residues implicated in PD-1-ITSM:Shp2-cSH2 interactions are altered in Shp1-
331 cSH2.

332 Given the very weak affinity of the Shp1-cSH2 domain with the ITSM of both PD-1 and BTLA, we
333 propose that receptors that stably recruit Shp1 must contain a strong docking site for Shp1-nSH2, such
334 as the BTLA-ITIM (**Fig. 6a**,**b**). The PD-1-ITIM, however, might be too weak to support stable, bivalent
335 PD-1:Shp1 binding. Moreover, because Shp1-nSH2 can bind intramolecularly to its catalytic domain to
336 inhibit its PTPase activity[52,53], a stronger ITIM might also allow the receptor to more efficiently release
337 the auto-inhibition of Shp1.

338 Biochemical research on PD-1 has led to a consensus that ITSM is its primary docking site for
339 Shp2[12,14,23,35,36]. Along this line, the current study shows that PD-1 uses ITSM to prefer Shp2 over Shp1
340 (**Fig. 3a**,**b**). Thus, ITSM is the ‘dominant hand’ of PD-1. In contrast, the ‘dominant hand’ of BTLA

341 appears to be its ITIM. Our data shows that ITIM of BTLA serves as the primary docking site for Shp1,
342 and allows BTLA to discriminate between Shp1 and Shp2 (**Fig. 6a**,**b**).

343 SH2 binding is contributed by both pY and its flanking residues[54,55]. Alanine is conserved at pY+1
344 position in the ITIMs of numerous immunoreceptors (**Extended Data Fig. 5**), suggesting its critical role
345 in the physiological functions of these receptors. In this sense, PD-1 is an interesting exception: its ITIM
346 appears the only ITIM that has a glycine at pY+1 position (**Extended Data Fig. 5**). Our study
347 demonstrates that the pY+1 glycine inhibits Shp1 recruitment, and a single replacement of glycine to an
348 alanine, valine, leucine or isoleucine was sufficient to induce PD-1:Shp1 association in T cells (**Figs. 8**
349 and **9**). These results suggest that a medium-sized nonpolar residue at pY+1 position is a defining
350 feature of a Shp1-docking site, specifically its nSH2 domain.

351 How could an alanine at pY+1 contribute to SH2 binding? In a reported crystal structure of NKG2A-
352 ITIM:Shp1-cSH2 complex (PDB code: 2YU7), the methyl group of pY+1 alanine form hydrophobic
353 contacts with nonpolar groups next to the pY-binding pocket within Shp1-cSH2. We speculate that
354 similar methyl-mediated hydrophobic contacts likely stabilize BTLA-ITIM:Shp1-nSH2 interactions. A
355 glycine at pY+1, as occurs in human PD-1-ITIM, likely prohibits such hydrophobic interactions due to
356 the lack of a methyl group in its side chain. Leucine and isoleucine might further promote the interaction
357 due to the more methyl groups in their side chains. Alternatively, the size of the pY+1 side chain might
358 dictate the strength of the hydrophobic contact, a medium-sized residue (leucine, isoleucine, valine or
359 alanine) might optimize the contact, whereas a small (glycine) or a bulky residue (phenylalanine or
360 tryptophan) would inhibit the interaction due to a steric effect. Structural studies will be needed to
361 definitively test these notions.

362 The result that leucine or isoleucine at pY+1 position enabled the most Shp1 recruitment (**Fig. 9**)
363 suggests that the alanine-containing, naturally-occurring ITIMs are suboptimal for recruitment of Shp1,
364 and modulating the side chain volume of pY+1 residue of ITIM may offer a means to tune Shp1 binding
365 activities in cell therapies. However suboptimal binding affinities may also implicate an important

366 regulatory role of the ITIM motif, for example a moderate level of Shp1/Shp2 recruitment may be
367 utilized in some contexts to restrict tonic inhibitory signaling and promote cell fitness[56]. More generally,
368 the diverse binding specificities of dual ITIM/ITSM motifs may enable more dynamic signaling pathways
369 that are essential for homeostasis of the immune system.

Acknowledgements

We thank P. Dennett and J. Zhang for critically reading the manuscript. T. Masubuchi is supported by the Human Frontier Science Program postdoctoral fellowship. This work was supported by R37 CA239072 from the National Institute of Health, a Searle Scholar Award from the Kinship Foundation, a Pew Biomedical Scholar Award from the Pew Charitable Trusts to E. Hui.

Author contributions

X.X., T.M., and E.H. designed the project. X.X., T.M. and Y.Z. generated plasmids, proteins and cell lines. X.X. conducted the co-IP experiments. T.M. conducted the cell-SLB assays, SPR experiments, and single molecule imaging. X.X., T.M., and E.H. wrote the manuscript.

Declaration of interests

The authors declare no competing financial interest.

385 **Methods**

386 **Reagents**

387 Biotin anti-human CD3ε (clone OKT3, BioLegend, #317320), human PD-L1-His (Sino Biological, #10084-
388 H08H), human ICAM-1-His (Sino Biological, #10346-H08H), and streptavidin (Invitrogen, #S888) were
389 used to functionalize SLBs. Anti-Shp1 (Life Technologies, #3H20L13), anti-Shp2 (BD Biosciences,
390 #101720), and F (ab') 2-Goat anti-Rabbit IgG (H+L) secondary antibody, alexa fluor 568 (Invitrogen,
391 #A21069) were used in the immunostaining for the cell-SLB assays. Anti-Phosphotyrosine (clone pY20,
392 Sigma-Aldrich, #P4110-1MG), anti-GFP (Invitrogen, #A-6455), anti-Shp1 (Proteintech, #24546-1-AP),
393 anti-Shp2 (Santa Cruz Biotechnology, #sc-7384), and Anti-GAPDH (Proteintech, #10494-1-AP) were
394 used in western blots. Phycoerythrin (PE) anti-human BTLA (clone MIH26, BioLegend, #344505) and
395 Pacific Blue anti-human PD-1 (clone EH12.2H7, BioLegend, #329916), were used in the staining of
396 Jurkat or Raji cells for flow cytometry.

397 **Cell cultures**

398 HEK293T cells were maintained in DMEM medium (Genesee Scientific, #25-501) supplemented with
399 10% fetal bovine serum (Omega Scientific, #FB-02) and 1% 100 × Penicillin-Streptomycin (GE
400 Healthcare, #SV30010) at 37 °C / 5% CO_2. Jurkat and Raji cells were maintained in RPMI-1640 medium
401 (Corning, #10-041-CM) supplemented with 10% fetal bovine serum, 100 U/mL of Penicillin, and 100
402 μg/mL of Streptomycin) at 37 °C / 5% CO_2.

403 **Recombinant proteins**

404 For SPR assays in **Figs. 3a** and **6a**, human $BTLA^{ICD}$ (aa 190-289), human $PD\text{-}1^{ICD}$ (aa 194-288), and
405 their tyrosine mutants ($BTLA^{FFYF}$, $BTLA^{FFFY}$, $PD\text{-}1^{FY}$, $PD\text{-}1^{YF}$) were expressed with an N-terminal His_{10} tag
406 in *Escherichia coli* using the pET28A vector, and purified using Ni-NTA agarose (ThermoFisher, #88223)
407 as described[24]. His_{10} tagged human protein tyrosine kinase Fyn was expressed in the Bac-to-Bac

408 baculovirus system and purified using Ni-NTA agarose. SNAP-Shp1-nSH2, SNAP-Shp1-nSH2, SNAP-
409 Shp2-nSH2, and SNAP-Shp2-cSH2 were expressed with an N-terminal GST tag followed by a
410 PreScission recognition sequence (LEVLFQGP), in *Escherichia coli* via the pGEX6p-2 vector. For the
411 single molecule imaging assay in **Extended Data Fig. 2**, all proteins were expressed with an N-terminal
412 GST tag followed by a PreScission recognition sequence (LEVLFQGP), in *Escherichia coli* via the
413 pGEX6p-2 vector. These included SNAP-Shp1-tSH2, SNAP-Shp2-tSH2, as well as the ICD of PD-1 WT
414 or its tyrosine mutants fused with an N terminal Avi-tag (GLNDIFEAQKIEWHE) and a C-terminal SNAPf
415 tag (Avi-PD-1^{YY}-SNAPf, Avi-PD-1^{FY}-SNAPf, Avi-PD-1^{YF}-SNAPf). All GST fusion proteins were purified
416 using Glutathione Agarose 4B (Gold Biotechnology, #G-250-50), and eluted with HEPES buffered saline
417 (HBS, 50 mM HEPES, 150 mM NaCl, 0.5 mM TCEP (Gold Biotechnology, #TCEP10), pH 7.5) containing
418 20 units/mL 3C protease to remove the GST tag. After elution, SNAP-Shp1-tSH2, SNAP-Shp2-tSH2 were
419 further labeled with SNAP ligand-JF646 (Janelia Research Campus (HHMI), #Janelia 2014-013) at 4 °C
420 overnight. Avi-PD-1^{YY}-SNAPf, Avi-PD-1^{FY}-SNAPf, Avi-PD-1^{YF}-SNAPf were further labeled with SNAP
421 ligand-JF549 (Janelia Research Campus (HHMI), #Janelia 2014-013) and biotin in the presence of 1 mM
422 Biotin (Sigma-Aldrich, #B4501), 1 μM BirA and 10 mM ATP (Gold Biotech, #A-081-100) at 4 °C overnight.
423 All affinity-purified proteins were subjected to gel filtration chromatography using HBS containing 10%
424 glycerol and 1 mM TCEP. The monomer fractions were pooled, snap frozen and stored at - 80 °C in small
425 aliquots. Gel filtration standards (Bio-Rad, #1511901) were run to confirm the sizes of eluted proteins.

426 **Phosphorylation of recombinant PD-1 and BTLA ICD proteins**

427 Purified His$_{10}$-PD-1, His$_{10}$-BTLA and Avi-PD-1-SNAPf proteins were incubated with 50 nM purified Fyn,
428 2 mM ATP, and 10 mM Na_3VO_4 at RT for 6 hours to achieve full phosphorylation, as indicated by the
429 complete shift of electrophoretic mobility on sodium dodecyl sulfate polyacrylamide gel electrophoresis
430 (SDS-PAGE). Monomeric form of these pre-phosphorylated proteins were purified using gel filtration
431 chromatography in HBS containing 10% glycerol and 1 mM TCEP, and stored in - 80 °C in aliquots.

432 **Shp2 antibody labeling**

433 For fluorescent staining of Shp2 in T cells, anti-Shp2 was fluorescently labeled using Alexa Fluor 647
434 NHS ester (ThermoFisher, #A37573), and unreacted chemicals were removed using Zeba Spin Desalting
435 Columns (ThermoFisher, #89890) following manufacturer's instructions.

436 **Cell lines**

437 Jurkat E6.1 cells were provided by Dr. Arthur Weiss (University of California San Francisco). HEK293T
438 cells and Raji cells were provided by Dr. Ronald Vale (University of California San Francisco). Shp2 KO
439 Jurkat, Shp1/Shp2 DKO Jurkat, Raji (PD-L1-mCherry), Raji (HVEM-mRuby2), Shp2 KO Raji (PD-L1-
440 mCherry), and Shp2 KO Raji (HVEM-mRuby2) cells were generated in our previous study[24]**.** Each gene
441 of interest was introduced into Jurkat cells via lentiviral transduction, as described previously[24]. Briefly,
442 each cDNA was cloned into a pHR vector backbone, and co-transfected with pMD2.G and psPAX2
443 packaging plasmids into HEK293T cells using polyethylenimine (PEI, Fisher Scientific, #NC1014320).
444 Virus-containing supernatants were harvested at 60-72 h post-transfection. WT Jurkat cells, Shp2 KO
445 Jurkat cells and Shp1/Shp2 DKO Jurkat cells were resuspended with the desired virus supernatant,
446 centrifuged at 35 °C, 1000 × g for 30 min, and incubated overnight at 37 °C, 5% CO2 before replacing
447 the virus supernatant with complete RPMI-1640 medium.

448 **Jurkat-Raji co-culture assay and immunoprecipitation**

449 For **Figs. 1**, **2a**, **4c**, **5b**, **7b**, **8b**, **8e**, **Extended Data Figs. 3b** and **4b**, Jurkat cells were starved in serum
450 free RPMI medium at 37 °C for 3 h prior to co-culture. Raji cells were pre-incubated with 30 ng/mL SEE
451 (Toxin Technologies, #ET404) in RPMI medium for 30 min at 37 °C. In order to avoid Shp2 competition
452 from Raji cells, Shp2 KO Raji cells were used in **Figs. 4c**, **7b**, **8b**, **8e** and **Extended Data Fig. 4b**.
453 Afterwards, four million SEE-loaded Raji cells and four million Jurkat cells were precooled on ice and
454 mixed in a 96-well plate. After centrifugation at 300 × g for 1 min at 4 °C to initiate Raji-Jurkat contact,
455 cells were immediately transferred to a 37 °C water bath. At 5 min or the time points indicated in the
456 figures, Raji-Jurkat conjugates were lysed with HBS containing 5% glycerol, detergent (1% NP-40),

457 protease inhibitor (1 mM PMSF), and phosphatase inhibitors (10 mM Na_3VO_4 and 10 mM NaF). GFP-
458 tagged PD-1 variants or BTLA variants were IP'ed from the lysate using GFP-Trap (Chromotek, #gta-20).
459 Equal fractions of the IP samples were subjected to SDS-PAGE and blotted with indicated antibodies.

460 **Flow cytometry**

461 Flow cytometry was conducted in an LSRFortessa cell analyzer (BD Biosciences). For **Fig. 5a**, **Extended**
462 **Data Figs. 1**, **3a** and **4a**, indicated Jurkat cells were washed with PBS and analyzed after staining with
463 PE anti-human BTLA (MIH26) or Pacific Blue anti-human PD-1 (EH12.2H7). For **Extended Data Fig. 1b**,
464 mCherry levels were measured using a FACSAria cell sorter (BD Biosciences) due to a lack of 561 nm
465 laser in the LSRFortessa cell analyzer. Data analyzed using FlowJo (FlowJo, LLC).

466 **SLB preparation and functionalization**

467 SLBs were formed on glass-bottomed 96-well plate (DOT Scientific Inc, #MGB096-1-2-LG-L). Briefly, the
468 plate was cleaned with 2.5 % Hellmanex (Sigma-Aldrich, #Z805939-1EA), etched with 5N NaOH, and
469 used for SLB formation as previously described [57]. Briefly, small unilamellar vesicles (SUVs) derived from
470 dried lipid film containing 95.5% POPC (Avanti Polar Lipids, #850457C), 2% biotin-DPPE (Avanti Polar
471 Lipids, #870285P), 2% DGS-NTA-Ni (Avanti Polar Lipids, #790404C) and 0.1% PEG 5000-PE (Avanti
472 Polar Lipids, #880230C) were added onto freshly treated plates to form SLBs. The SLBs were rinsed with
473 wash buffer (1x PBS containing 0.1% BSA) and mixed with 1 μg/mL streptavidin, 0.1 nM His-tagged
474 human PD-L1 ectodomain, and 3 nM His-tagged human ICAM-1 ectodomain at 37 °C for 1 h. Afterward,
475 the SLBs were rinsed with wash buffer and further incubated with 5 μg/mL biotin anti-human-CD3ε at
476 37 °C for 30 min, followed by three rinses with wash buffer and three rinses with imaging buffer (20 mM
477 HEPES pH 7.5, 137 mM NaCl, 5 mM KCl, 1 mM $CaCl_2$, 2 mM $MgCl_2$, 0.7 mM Na_2HPO_4, 6 mM D-Glucose).

478 **Cell-SLB image acquisition and analysis**

479 Jurkat cells were resuspended in imaging buffer and overlaid onto freshly formed PD-L1/ICAM/Okt3-

480 functionalized SLBs. After 5 min incubation at 37 °C, SLB-bound cells were overlaid with 2%
481 paraformaldehyde (PFA, Fisher Scientific, #50980494), and incubated at room temperature (RT) for 15
482 min for fixation. SLB-associated, PFA-treated cells were washed with blocking buffer (1x PBS containing
483 3% BSA), and permeabilized with 1x PBS containing 3% BSA and 0.1% Saponin at RT for 30 min. To
484 observe mCherry-tagged $Shp1^{WT}$ or domain swapping mutants (**Fig. 4b**), cells were directly imaged at
485 both GFP (488 nm) and mCherry (561 nm) channels. To observe endogenous Shp2 (**Fig. 2b**), the
486 permeabilized cells were stained with Alexa-Fluor-647-labeled anti-Shp2 at 4 °C for 16 hours, followed
487 by fixation with 4% PFA. To observe endogenous Shp1 (**Figs. 7c**, **8c**, **8f**, and **9a**), the permeabilized cells
488 were stained with anti-Shp1 at 4 °C for 16 hours, followed by fixation with 4% PFA, and further staining
489 with Alexa-Fluor-568-labeled anti-rabbit IgG at RT for 1 hour and another treatment with 4% PFA. The
490 fluorescent cell images were acquired on a Nikon Eclipse Ti TIRF microscope equipped with a 100x Apo
491 TIRP 1.49 NA objective lens, controlled by the Micro-Manager software[58]. Fiji[59] was used to quantify the
492 degree of recruitment of Shp1 and Shp2 to PD-1 microclusters. Mask images identifying the area of PD-
493 1 microclusters were generated by applying the "subtract background" command to PD-1 (mGFP) images
494 using the default setting. The fluorescent signals of anti-Shp1, anti-Shp2 and PD-1 (GFP) in the masked
495 overlaid images were measured, and used to calculate the anti-Shp1 FI/GFP FI ratio and Shp2/PD-1
496 ratio for each cell.

497 **Surface plasmon resonance (SPR) assay**

498 For **Figs. 3a** and **6a**, direct interaction between individual SH2 (nSH2 or cSH2) of Shp1 or Shp2 and
499 BTLA ICD, PD-1 ICD, or their tyrosine mutants ($BTLA^{FFYF}$, $BTLA^{FFFY}$, $PD\text{-}1^{FY}$, $PD\text{-}1^{YF}$) was monitored by
500 OpenSPR (Nicoya) equipped with Ni sensor chip (Nicoya, #SEN-AU-100-10-NTA). Pre-phosphorylated
501 His_{10}-tagged PD-1 ICD or BTLA ICD was immobilized onto a Ni sensor chip to achieve approximately
502 1500 RU by following the Ni sensor wizard in OpenSPR software. SH2 of interest was diluted in running
503 buffer (20 mM HEPES, 150 mM NaCl, 5 mM Imidazole (Sigma-Aldrich, #I202), 0.05 % Tween-20, 10 %
504 Glycerol, pH 7.5), and injected. The association and dissociation phases of SH2 were monitored at flow
505 rate of 20 μL/min. The Ni sensor chip was regenerated with 50 mM NaOH before injecting the next SH2.

506 Sensorgrams were analyzed using the “Evaluate EC50” method in TraceDrawer software (Ridgeview
507 Instruments).

508 **Single molecule imaging assay**

509 For **Extended Data Fig. 2**, surface-passivated coverslips and slide glasses used in single molecule
510 imaging assays were prepared and assembled as previously described[60]. Surface-passivated glass
511 chambers were incubated with blocking buffer (50 mM HEPES, 150 mM NaCl, 0.1 % BSA) at RT for 5
512 min and with 0.5 μM Streptavidin in blocking buffer at RT for 5 min, followed by two washes with blocking
513 buffer. The glass chambers were further incubated with 10 pM pre-phosphorylated, biotinylated, JF549-
514 labeled PD-1^{YY}, PD-1^{FY}, or PD-1^{YF}, and incubate at RT for 5 min. The unbound proteins were removed
515 with blocking buffer and JF646-labeled SH2 proteins were injected to the chambers. The fluorescent
516 images were acquired at 20 Hz on a Nikon Eclipse Ti TIRF microscope equipped with a 100x Apo TIRP
517 1.49 NA objective lens, controlled by the Micro-Manager software[58].

518 **Fluorescent intensity distribution analysis and photobleaching analysis**

519 For **Extended Data Fig. 2c**,**d**, JF646-labeled PD-1 attached on coverslips were illuminated with the 50
520 mW 488 nm laser for photobleaching observation. The initial positions of fluorescent spots for JF646-
521 labeled PD-1 were determined by the “ThunderSTORM” plugin [61] in Fiji. The fluorescent intensities at
522 each determined position in initial images were measured and plotted into histogram fit with Gaussian
523 distributions, and those of whole image stacks were measured for fluorescent trajectories.

524 **Fluorescent trajectory analysis and colocalization analysis**

525 For **Extended Data Fig. 2d**,**f**, the positions of fluorescent spots for JF549-labeled PD-1 were determined
526 by the “ThunderSTORM” plugin in Fiji. Likewise, the fluorescent movies for JF646-labeled tSH2 proteins
527 were Z-projected to “maximum intensity” and analyzed by the “ThunderSTORM” plugin to determine the
528 positions where tSH2 proteins bound. The positions detected in both JF549 and JF646 channels were

529 determined as spots representing PD-1 molecules that recruited tSH2 protein at any given time during
530 the image acquisition. The fluorescent intensities of JF646 within those areas were measured to
531 fluorescent trajectories of tSH2 proteins. The bound and unbound states of tSH2 proteins in the
532 fluorescent trajectories were estimated with Hidden Markov Model in a custom written Python script. The
533 colocalization rates of PD-1 and tSH2 protein were calculated by dividing the total number of PD-1 spots
534 by the number of PD-1 spots that recruited SH2 proteins within 0.5 seconds of image acquisitions.

535 **Quantification and statistical analysis**

536 Data were shown as mean ± s.d., and number of replicates were indicated in figure legends. Curve fitting
537 and normalization were performed in GraphPad Prism 8 (GraphPad). Statistical significance was
538 evaluated by Student's t-test (*, $p < 0.05$; **, $p < 0.01$; ***, $p < 0.001$; ****, $p < 0.0001$; ns, not significant).
539 Data with $p < 0.05$ are considered statistically significant.

540

541 **References:**

542 1. Sadowski, I., Stone, J.C. & Pawson, T. A noncatalytic domain conserved among cytoplasmic protein-
543 tyrosine kinases modifies the kinase function and transforming activity of Fujinami sarcoma virus
544 P130gag-fps. *Mol Cell Biol* **6**, 4396-408 (1986).
545 2. Waksman, G. et al. Crystal structure of the phosphotyrosine recognition domain SH2 of v-src complexed
546 with tyrosine-phosphorylated peptides. *Nature* **358**, 646-53 (1992).
547 3. Denu, J.M. & Dixon, J.E. Protein tyrosine phosphatases: mechanisms of catalysis and regulation. *Curr*
548 *Opin Chem Biol* **2**, 633-41 (1998).
549 4. Paul, S. & Lombroso, P.J. Receptor and nonreceptor protein tyrosine phosphatases in the nervous
550 system. *Cell Mol Life Sci* **60**, 2465-82 (2003).
551 5. Tonks, N.K. Protein tyrosine phosphatases: from genes, to function, to disease. *Nat Rev Mol Cell Biol* **7**,
552 833-46 (2006).
553 6. Senis, Y.A. Protein-tyrosine phosphatases: a new frontier in platelet signal transduction. *J Thromb*
554 *Haemost* **11**, 1800-13 (2013).
555 7. Veillette, A., Bookman, M.A., Horak, E.M. & Bolen, J.B. The CD4 and CD8 T cell surface antigens are
556 associated with the internal membrane tyrosine-protein kinase p56lck. *Cell* **55**, 301-8 (1988).
557 8. Barber, E.K., Dasgupta, J.D., Schlossman, S.F., Trevillyan, J.M. & Rudd, C.E. The CD4 and CD8 antigens are
558 coupled to a protein-tyrosine kinase (p56lck) that phosphorylates the CD3 complex. *Proc Natl Acad Sci U*
559 *S A* **86**, 3277-81 (1989).
560 9. Ley, S.C., Marsh, M., Bebbington, C.R., Proudfoot, K. & Jordan, P. Distinct intracellular localization of Lck
561 and Fyn protein tyrosine kinases in human T lymphocytes. *J Cell Biol* **125**, 639-49 (1994).

562 10. Courtney, A.H., Lo, W.L. & Weiss, A. TCR Signaling: Mechanisms of Initiation and Propagation. *Trends*
563 *Biochem Sci* **43**, 108-123 (2018).
564 11. Esensten, J.H., Helou, Y.A., Chopra, G., Weiss, A. & Bluestone, J.A. CD28 Costimulation: From Mechanism
565 to Therapy. *Immunity* **44**, 973-88 (2016).
566 12. Chemnitz, J.M., Parry, R.V., Nichols, K.E., June, C.H. & Riley, J.L. SHP-1 and SHP-2 associate with
567 immunoreceptor tyrosine-based switch motif of programmed death 1 upon primary human T cell
568 stimulation, but only receptor ligation prevents T cell activation. *J Immunol* **173**, 945-54 (2004).
569 13. Gavrieli, M., Watanabe, N., Loftin, S.K., Murphy, T.L. & Murphy, K.M. Characterization of
570 phosphotyrosine binding motifs in the cytoplasmic domain of B and T lymphocyte attenuator required
571 for association with protein tyrosine phosphatases SHP-1 and SHP-2. *Biochem Biophys Res Commun* **312**,
572 1236-43 (2003).
573 14. Okazaki, T., Maeda, A., Nishimura, H., Kurosaki, T. & Honjo, T. PD-1 immunoreceptor inhibits B cell
574 receptor-mediated signaling by recruiting src homology 2-domain-containing tyrosine phosphatase 2 to
575 phosphotyrosine. *Proc Natl Acad Sci U S A* **98**, 13866-71 (2001).
576 15. Watanabe, N. et al. BTLA is a lymphocyte inhibitory receptor with similarities to CTLA-4 and PD-1. *Nature*
577 *Immunology* **4**, 670-9 (2003).
578 16. Freeman, G.J. et al. Engagement of the PD-1 immunoinhibitory receptor by a novel B7 family member
579 leads to negative regulation of lymphocyte activation. *J Exp Med* **192**, 1027-34 (2000).
580 17. Latchman, Y. et al. PD-L2 is a second ligand for PD-1 and inhibits T cell activation. *Nature Immunology* **2**,
581 261-8 (2001).
582 18. Dong, H., Zhu, G., Tamada, K. & Chen, L. B7-H1, a third member of the B7 family, co-stimulates T-cell
583 proliferation and interleukin-10 secretion. *Nat Med* **5**, 1365-9 (1999).
584 19. Sedy, J.R. et al. B and T lymphocyte attenuator regulates T cell activation through interaction with
585 herpesvirus entry mediator. *Nature Immunology* **6**, 90-8 (2005).
586 20. Compaan, D.M. et al. Attenuating lymphocyte activity: the crystal structure of the BTLA-HVEM complex.
587 *J Biol Chem* **280**, 39553-61 (2005).
588 21. Gonzalez, L.C. et al. A coreceptor interaction between the CD28 and TNF receptor family members B and
589 T lymphocyte attenuator and herpesvirus entry mediator. *Proc Natl Acad Sci U S A* **102**, 1116-21 (2005).
590 22. Hui, E. et al. T cell costimulatory receptor CD28 is a primary target for PD-1-mediated inhibition. *Science*
591 **355**, 1428-1433 (2017).
592 23. Yokosuka, T. et al. Programmed cell death 1 forms negative costimulatory microclusters that directly
593 inhibit T cell receptor signaling by recruiting phosphatase SHP2. *J Exp Med* **209**, 1201-17 (2012).
594 24. Xu, X. et al. PD-1 and BTLA regulate T cell signaling differentially and only partially through SHP1 and
595 SHP2. *J Cell Biol* **219**(2020).
596 25. Coxon, C.H., Geer, M.J. & Senis, Y.A. ITIM receptors: more than just inhibitors of platelet activation.
597 *Blood* **129**, 3407-3418 (2017).
598 26. Crocker, P.R., Paulson, J.C. & Varki, A. Siglecs and their roles in the immune system. *Nat Rev Immunol* **7**,
599 255-66 (2007).
600 27. Riley, J.L. PD-1 signaling in primary T cells. *Immunol Rev* **229**, 114-25 (2009).
601 28. Wu, N. & Veillette, A. SLAM family receptors in normal immunity and immune pathologies. *Curr Opin*
602 *Immunol* **38**, 45-51 (2016).
603 29. Lorenz, U. SHP-1 and SHP-2 in T cells: two phosphatases functioning at many levels. *Immunol Rev* **228**,
604 342-59 (2009).
605 30. Brockdorff, J., Williams, S., Couture, C. & Mustelin, T. Dephosphorylation of ZAP-70 and inhibition of T
606 cell activation by activated SHP1. *European Journal of Immunology* **29**, 2539-50 (1999).
607 31. Mintz, M.A. et al. The HVEM-BTLA Axis Restrains T Cell Help to Germinal Center B Cells and Functions as
608 a Cell-Extrinsic Suppressor in Lymphomagenesis. *Immunity* (2019).
609 32. Celis-Gutierrez, J. et al. Quantitative Interactomics in Primary T Cells Provides a Rationale for
610 Concomitant PD-1 and BTLA Coinhibitor Blockade in Cancer Immunotherapy. *Cell Rep* **27**, 3315-3330 e7
611 (2019).

612 33. Goyette, J. et al. Biophysical assay for tethered signaling reactions reveals tether-controlled activity for
613 the phosphatase SHP-1. *Sci Adv* **3**, e1601692 (2017).
614 34. Xu, X. et al. BTLA and PD-1 employ distinct phosphatases to differentially repress T cell signaling. *BioRxiv*
615 (2019).
616 35. Peled, M. et al. Affinity purification mass spectrometry analysis of PD-1 uncovers SAP as a new
617 checkpoint inhibitor. *Proc Natl Acad Sci U S A* **115**, E468-E477 (2018).
618 36. Patsoukis, N. et al. Interaction of SHP-2 SH2 domains with PD-1 ITSM induces PD-1 dimerization and
619 SHP-2 activation. *Commun Biol* **3**, 128 (2020).
620 37. Marasco, M. et al. Molecular mechanism of SHP2 activation by PD-1 stimulation. *Sci Adv* **6**, eaay4458
621 (2020).
622 38. Avril, T., Floyd, H., Lopez, F., Vivier, E. & Crocker, P.R. The membrane-proximal immunoreceptor
623 tyrosine-based inhibitory motif is critical for the inhibitory signaling mediated by Siglecs-7 and -9, CD33-
624 related Siglecs expressed on human monocytes and NK cells. *J Immunol* **173**, 6841-9 (2004).
625 39. Sui, L. et al. IgSF13, a novel human inhibitory receptor of the immunoglobulin superfamily, is
626 preferentially expressed in dendritic cells and monocytes. *Biochem Biophys Res Commun* **319**, 920-8
627 (2004).
628 40. Alvarez-Errico, D. et al. IREM-1 is a novel inhibitory receptor expressed by myeloid cells. *European*
629 *Journal of Immunology* **34**, 3690-701 (2004).
630 41. Veillette, A., Thibaudeau, E. & Latour, S. High expression of inhibitory receptor SHPS-1 and its
631 association with protein-tyrosine phosphatase SHP-1 in macrophages. *J Biol Chem* **273**, 22719-28 (1998).
632 42. Paling, N.R. & Welham, M.J. Role of the protein tyrosine phosphatase SHP-1 (Src homology
633 phosphatase-1) in the regulation of interleukin-3-induced survival, proliferation and signalling. *Biochem J*
634 **368**, 885-94 (2002).
635 43. Ke, Y. et al. Deletion of Shp2 in the brain leads to defective proliferation and differentiation in neural
636 stem cells and early postnatal lethality. *Molecular and Cellular Biology* **27**, 6706-17 (2007).
637 44. Kuo, E. et al. Tyrosine phosphatases Shp1 and Shp2 have unique and opposing roles in oligodendrocyte
638 development. *J Neurochem* **113**, 200-12 (2010).
639 45. Gascoigne, N. et al. Themis and the control of SHP1 phosphatase activity in TCR signal strength during
640 thymocyte positive selection. *Journal of Immunology* **194**(2015).
641 46. Diestler, D.J. & Knapp, E.W. Statistical thermodynamics of the stability of multivalent ligand-receptor
642 complexes. *Phys Rev Lett* **100**, 178101 (2008).
643 47. Zhou, H.X. & Gilson, M.K. Theory of free energy and entropy in noncovalent binding. *Chem Rev* **109**,
644 4092-107 (2009).
645 48. Jackson, D.E., Kupcho, K.R. & Newman, P.J. Characterization of phosphotyrosine binding motifs in the
646 cytoplasmic domain of platelet/endothelial cell adhesion molecule-1 (PECAM-1) that are required for
647 the cellular association and activation of the protein-tyrosine phosphatase, SHP-2. *J Biol Chem* **272**,
648 24868-75 (1997).
649 49. Zhang, Y. et al. The Influence of Molecular Reach and Diffusivity on the Efficacy of Membrane-Confined
650 Reactions. *Biophys J* **117**, 1189-1201 (2019).
651 50. Clemens, L. et al. Determination of the molecular reach of the protein tyrosine phosphatase SHP-1.
652 *Biophys J* (2021).
653 51. Poole, A.W. & Jones, M.L. A SHPing tale: perspectives on the regulation of SHP-1 and SHP-2 tyrosine
654 phosphatases by the C-terminal tail. *Cell Signal* **17**, 1323-32 (2005).
655 52. Pei, D., Lorenz, U., Klingmuller, U., Neel, B.G. & Walsh, C.T. Intramolecular regulation of protein tyrosine
656 phosphatase SH-PTP1: a new function for Src homology 2 domains. *Biochemistry* **33**, 15483-93 (1994).
657 53. Yang, J. et al. Crystal structure of human protein-tyrosine phosphatase SHP-1. *J Biol Chem* **278**, 6516-20
658 (2003).
659 54. Pawson, T. Protein modules and signalling networks. *Nature* **373**, 573-80 (1995).
660 55. Kuriyan, J. & Cowburn, D. Modular peptide recognition domains in eukaryotic signaling. *Annu Rev*
661 *Biophys Biomol Struct* **26**, 259-88 (1997).

662 56. Fernandes, R.A. et al. Immune receptor inhibition through enforced phosphatase recruitment. *Nature*
663 **586**, 779-784 (2020).
664 57. Ahrends, T. et al. CD4(+) T Cell Help Confers a Cytotoxic T Cell Effector Program Including Coinhibitory
665 Receptor Downregulation and Increased Tissue Invasiveness. *Immunity* **47**, 848-+ (2017).
666 58. Edelstein, A.D. et al. Advanced methods of microscope control using muManager software. *J Biol*
667 *Methods* **1**(2014).
668 59. Schindelin, J. et al. Fiji: an open-source platform for biological-image analysis. *Nat Methods* **9**, 676-82
669 (2012).
670 60. Chandradoss, S.D. et al. Surface passivation for single-molecule protein studies. *J Vis Exp* (2014).
671 61. Ovesny, M., Krizek, P., Borkovec, J., Svindrych, Z. & Hagen, G.M. ThunderSTORM: a comprehensive
672 ImageJ plug-in for PALM and STORM data analysis and super-resolution imaging. *Bioinformatics* **30**,
673 2389-90 (2014).

674

675

676

677 **Figures and legends**

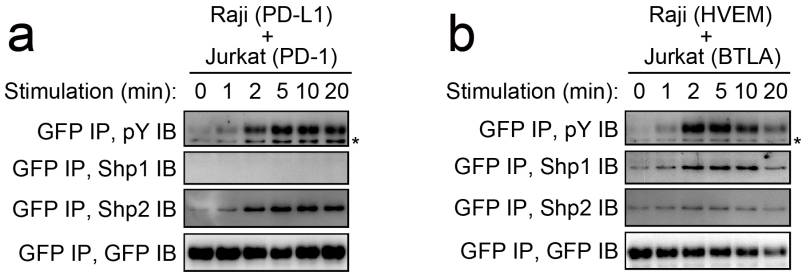

678

679 **Fig. 1: PD-1 recruits Shp2 but not Shp1, whereas BTLA prefers to recruit Shp1.**

680 Representative immunoblots (IBs) showing the levels of bound Shp1 and Shp2 in PD-1-mGFP (**a**) or
681 BTLA-mGFP (**b**) pulled down by GFP IP from indicated cell lysates, with the duration of stimulation
682 prior to lysis indicated (see Methods). IBs of GFP and pY of the same samples were shown to indicate
683 PD-1 or BTLA input and their degrees of phosphorylation.

684

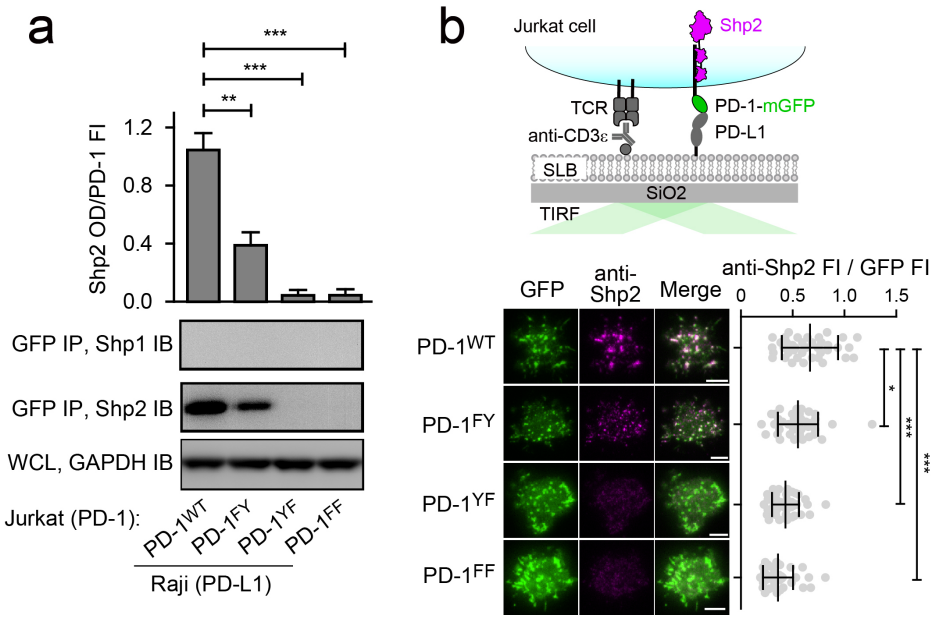

Fig. 2: Both ITIM and ITSM contribute to the ability of PD-1 to recruit Shp2.

a, Representative IBs showing the levels of Shp1 and Shp2 bound to mGFP-tagged PD-1 variants pulled down from the indicated co-culture lysates via GFP IP. GAPDH IB of the whole cell lysates (WCL) served as a loading control (see Methods). Bar graphs on top summarize Shp2 optical density (OD) normalized to the fluorescence intensity (FI) of each PD-1 variant, based on flow cytometry data in Extended Data Fig. 1a. Error bars are s.d. from three independent experiments. **b**, Upper, a cartoon depicting a PD-1-mGFP-expressing Jurkat cell in contact with an SLB containing anti-CD3ε and PD-L1^{ECD}. Lower left, representative TIRF images of both PD-1 (GFP) and endogenous Shp2 (stained with anti-Shp2) in an SLB-associated Jurkat expressing indicated PD-1 variants. Lower right, dot plots summarizing anti-Shp2 FI normalized to GFP FI of 40 Jurkat cells under each condition (see Methods); Error bars: s.d.. Scale bars: 5 μm. *P < 0.05; **P < 0.01; ***P < 0.001; ns, not significant; Student's t-test.

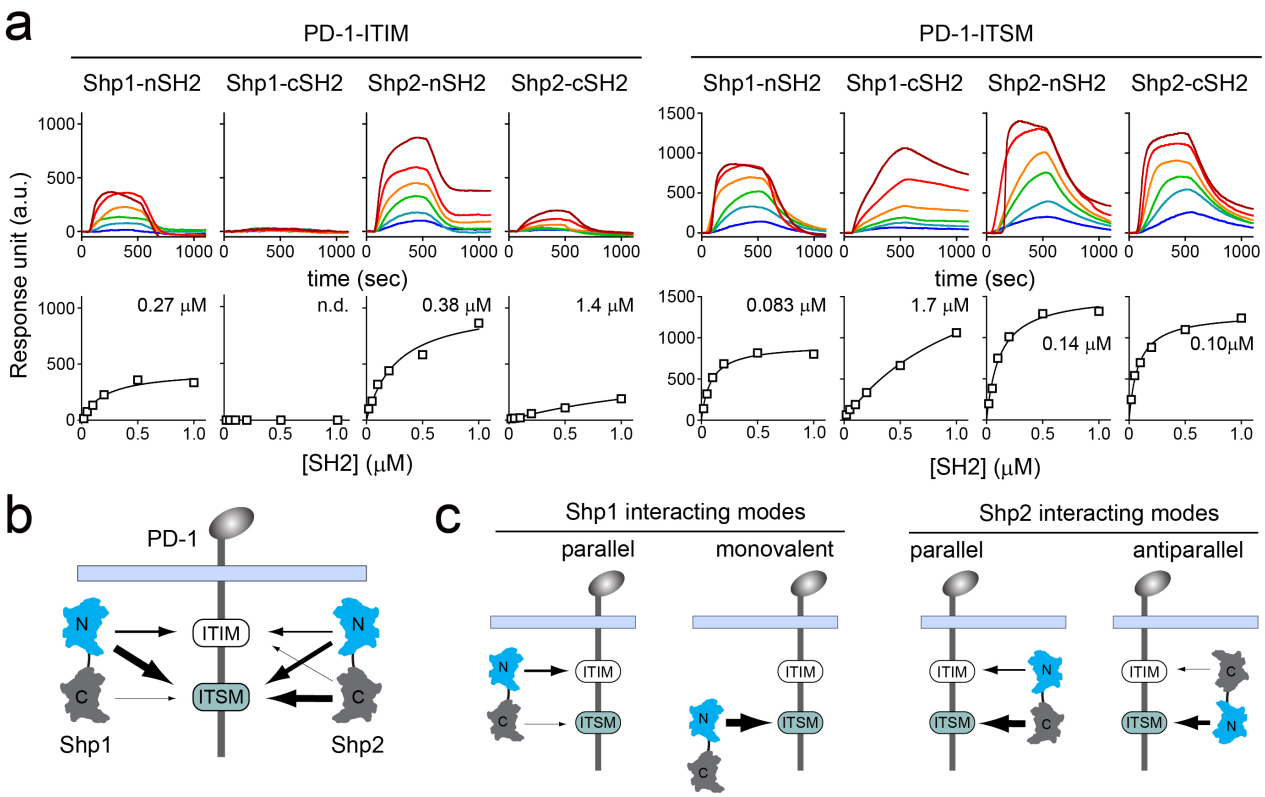

Fig. 3: SPR measurements of binding between individual SH2 of Shp1 or Shp2 and ITIM or ITSM of PD-1.

a, SPR sensorgrams (top) and the derived equilibrium binding curves (bottom) showing the interactions of indicated SH2 and phosphorylated PD-1-ITIM (PD-1 YF) or PD-1-ITSM (PD-1 FY) immobilized onto Ni sensor chips. Individual SH2 proteins were injected at 20, 50, 100, 200, 500, 1000 nM. Shown are representative of three independent experiments. The calculated K_d values are indicated in the binding curves. **b**, A cartoon depicting relative binding affinities of Shp1/Shp2 individual SH2 to PD-1-ITIM/ITSM, with the thickness of arrows matching the relative affinities calculated from the SPR data. **c**, Possible interacting modes of Shp1/Shp2-tSH2 with PD-1.

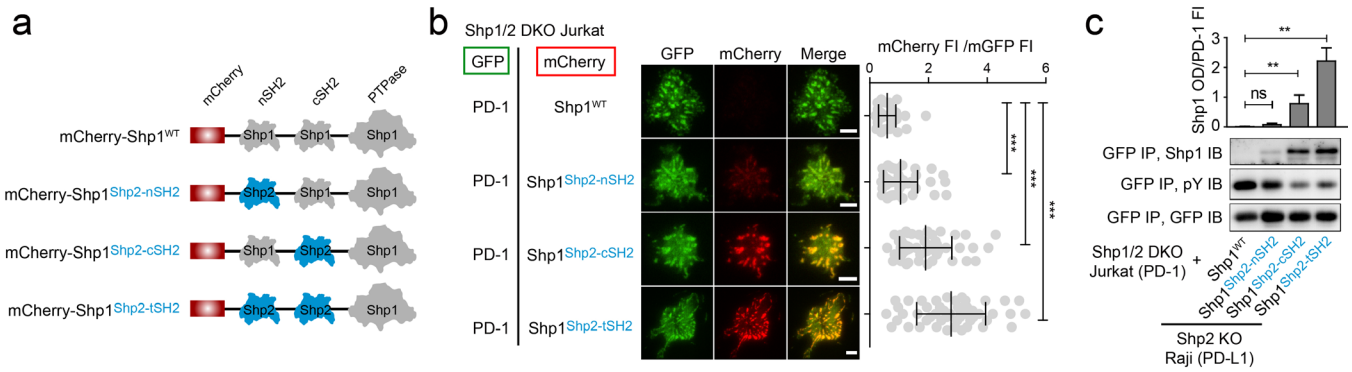

Fig. 4: Swapping the cSH2 of Shp1 with that of Shp2 induced PD-1:Shp1 association in T cells.

a, Diagram showing the design of mCherry-tagged, SH2-swapped Shp1 variants, with one or both of its SH2 replaced with that of Shp2. **b**, Left, representative TIRF images of PD-1 (GFP) and Shp1 variants (mCherry) in SLB-associated Shp1/Shp2 DKO Jurkat expressing PD-1-mGFP and mCherry-Shp1 variants. Right, dot plots summarizing mCherry FI normalized to GFP FI of 40 Jurkat cells under each condition. Error bars: s.d.. Scale bars: 5 μm. **c**, Representative IBs of mCherry-Shp1 variants co-precipitated with PD-1-mGFP from indicated cell lysates. IBs of GFP indicate PD-1 input. IBs of pY indicate PD-1 phosphorylation. Bar graphs summarize OD of Shp1 variants normalized to the FI of PD-1, based on flow cytometry data in Extended Data Fig.1b. Error bars are s.d. from three independent experiments. *P < 0.05; **P < 0.01; ns, not significant; Student's t-test.

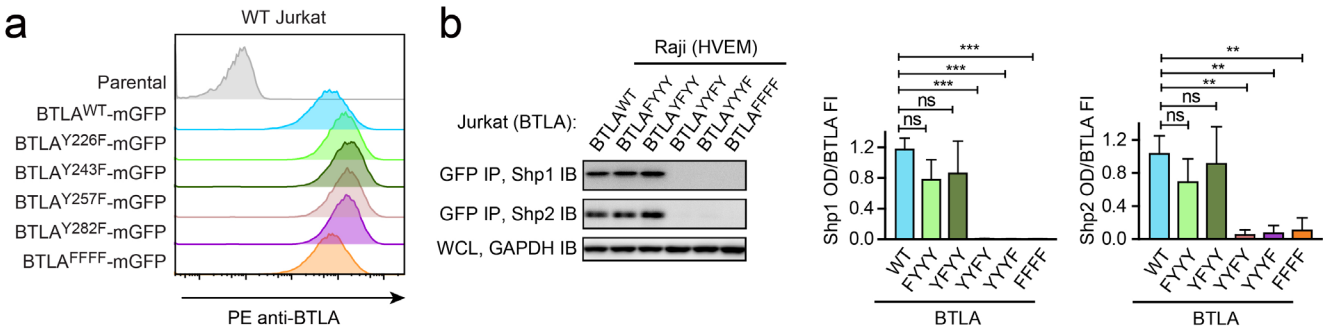

Fig. 5: Both ITIM and ITSM are required for BTLA to recruit Shp1/Shp2.

a, Flow cytometry histograms showing BTLA surface expressions in the indicated Jurkat cells. **b**, Left, representative IBs showing the levels of Shp1 and Shp2 bound to the mGFP-tagged BTLA variants captured by GFP IP. GAPDH IB of the WCL served as a loading control. Right, bar graphs summarizing Shp1 OD and Shp2 OD normalized to the FI of the corresponding BTLA variants, based on flow cytometry data in A. Error bars are s.d. of three independent experiments. **P < 0.01; ***P < 0.001; ns, not significant; Student's t-test (n = 3).

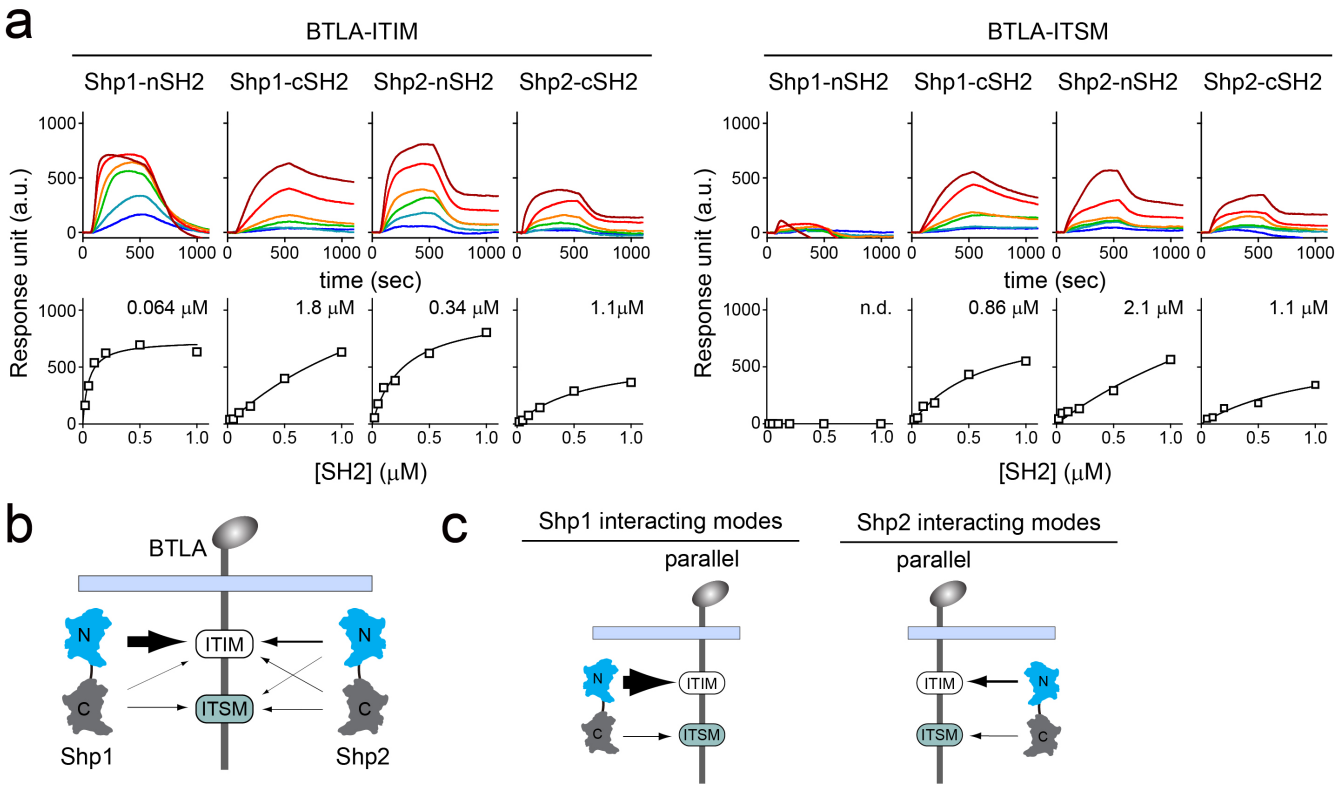

Fig. 6: SPR measurements of binding between individual SH2 of Shp1 or Shp2 and ITIM or ITSM of BTLA.

a, SPR sensorgrams (top) and the derived equilibrium binding curves (bottom) showing the interactions of indicated SH2 and phosphorylated BTLA-ITIM (BTLA FFYF) or BTLA-ITSM (BTLA FFFY) immobilized to Ni sensor chips. Individual SH2 proteins were injected at 20, 50, 100, 200, 500, 1000 nM. Shown are representative of three independent experiments. The calculated K_d values are indicated in the binding curves. **b**, A cartoon depicting relative binding affinities of Shp1/Shp2 individual SH2 to BTLA-ITIM/ITSM, with the thickness of arrows matching the relative affinities calculated from the SPR data in A. **c**, Possible interacting modes of Shp1/Shp2-tSH2 with BTLA.

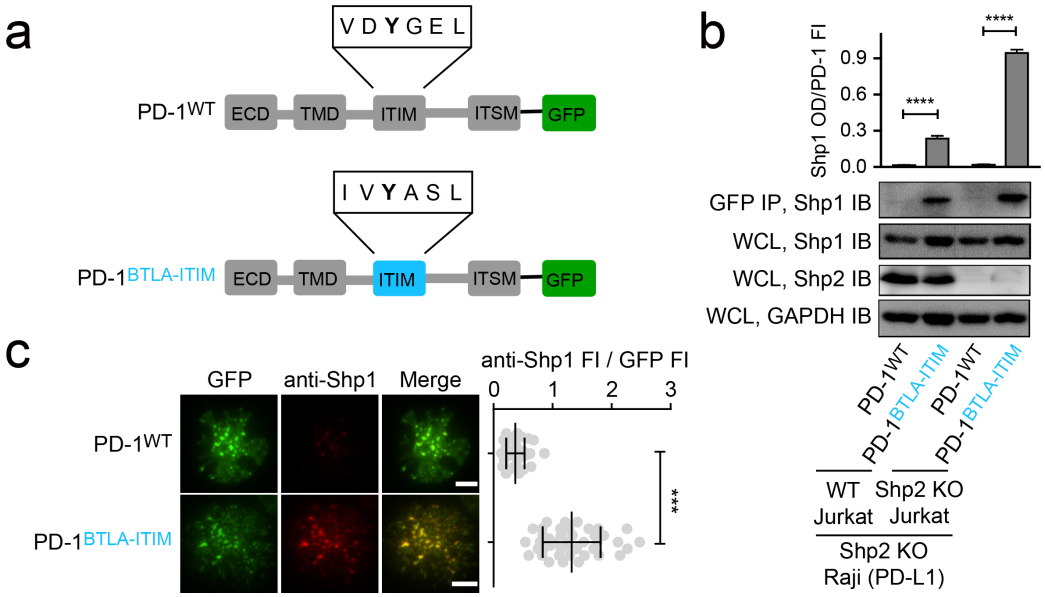

Fig. 7: Swapping PD-1-ITIM with BTLA-ITIM induced PD-1:Shp1 interaction in T cells.

a, Cartoons depicting the domains and motifs of PD-1^{WT}-mGFP and PD-1$^{BTLA\text{-}ITIM}$-mGFP. **b**, Representative IBs showing the levels of Shp1 bound to mGFP-tagged PD-1 variants pulled down from the indicated co-culture lysates via GFP IP. Shp1 IB and Shp2 IB of the WCL indicate their input. GAPDH IB of the WCL served as a loading control. Bar graphs summarize Shp1 OD normalized to the FI of each PD-1 variant, based on flow cytometry data in Extended Data Fig. 1c. Error bars are s.d. from three independent experiments. **c**, Left, representative TIRF images of both PD-1 (GFP) and endogenous Shp1 (stained with anti-Shp1) in an SLB-associated Shp2 KO Jurkat expressing indicated PD-1 variants. Right, dot plots summarizing anti-Shp1 FI normalized to GFP FI of 40 Jurkat cells under each condition; Error bars: s.d.. Scale bars: 5 μm. ***P < 0.001; ****P < 0.0001; Student's t-test.

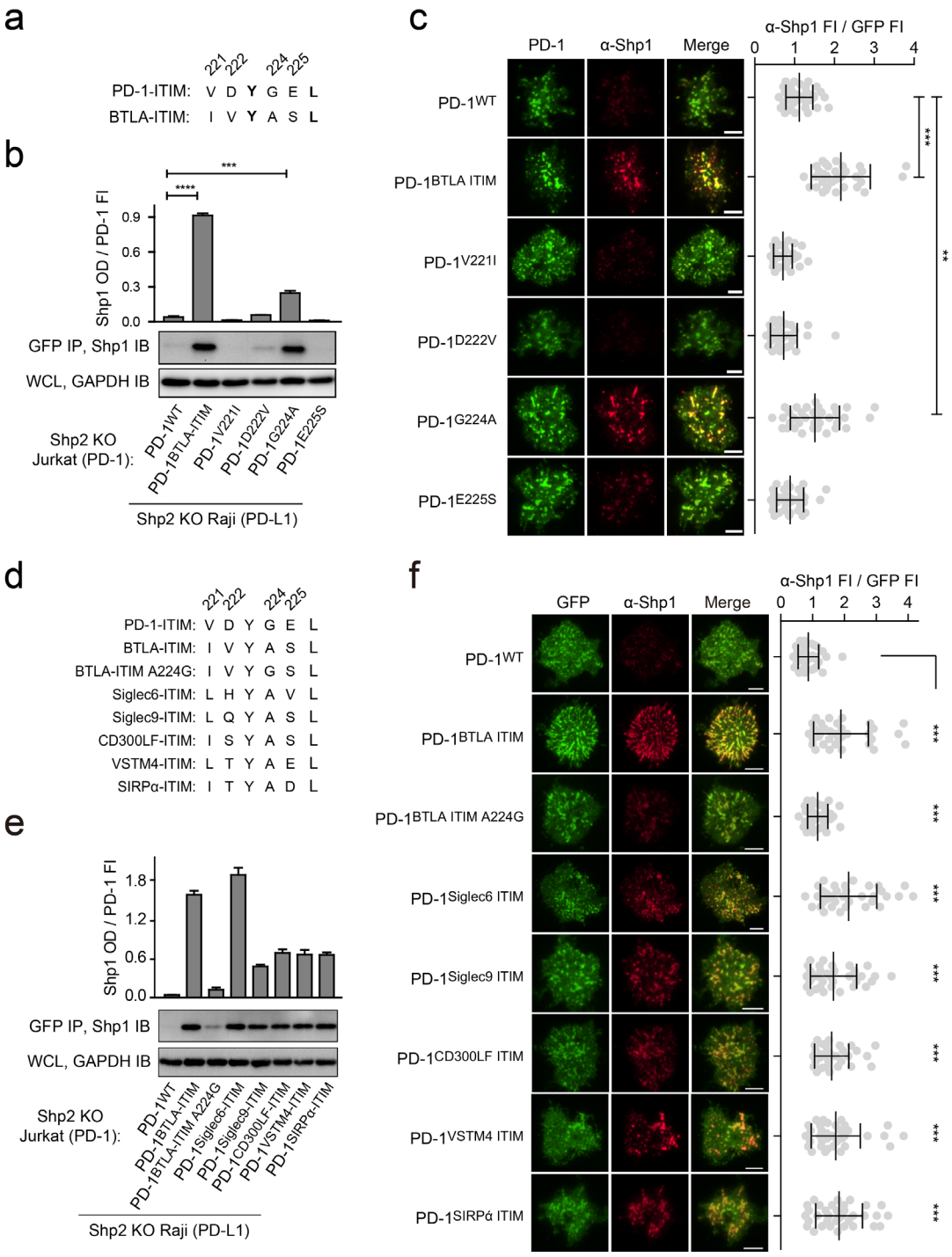

Fig. 8: Glycine to alanine substitution at the pY+1 position of PD-1 ITIM promoted Shp1 recruitment.

a, Cartoons depicting the amino acid (AA) alignment of PD-1-ITIM and BTLA-ITIM. **b**, Representative IBs showing the levels of Shp1 bound to mGFP-tagged PD-1 variants pulled down from the indicated co-culture lysates via GFP IP. GAPDH IB of WCL served as a loading control. Bar graphs summarize Shp1 OD normalized to the FI of each PD-1 variant, based on flow cytometry data in Extended Data Fig. 1d. Error bars are s.d. from three independent experiments. **c**, Left, representative TIRF images of both PD-1 (GFP) and endogenous Shp1 (stained with anti-Shp1) in an SLB-associated Shp2 KO Jurkat cell expressing indicated PD-1 variants. Right, dot plots summarizing anti-Shp1 FI normalized to GFP FI of 35 Jurkat cells under each condition (see Methods); Error bars: s.d.. Scale bars: 5 μm. **d**,

767 Cartoons showing the AA sequences of ITIM of indicated receptors. **e**, Representative IBs showing the
768 levels of Shp1 co-precipitated with mGFP-tagged PD-1 variants, with the original ITIM replaced by the
769 indicated ITIM, from the indicated co-culture lysates via GFP IP. GAPDH IB of WCL served as a
770 loading control. Bar graphs summarize Shp1 OD normalized to the FI of each PD-1 variant, based on
771 flow cytometry data in Extended Data Fig. 1e. Error bars are s.d. from three independent experiments.
772 **f**, Left, representative TIRF images of both PD-1 (GFP) and endogenous Shp1 (stained with anti-Shp1)
773 in an SLB-associated Shp2 KO Jurkat cell expressing PD-1 variants with indicated ITIM. Right, dot
774 plots summarizing anti-Shp1 FI normalized to GFP FI of 35 Jurkat cells under each condition (see
775 Methods); Error bars: s.d.. Scale bars: 5 μm.
776 **P < 0.01; ***P < 0.001; ****P < 0.0001; Student's t-test

777

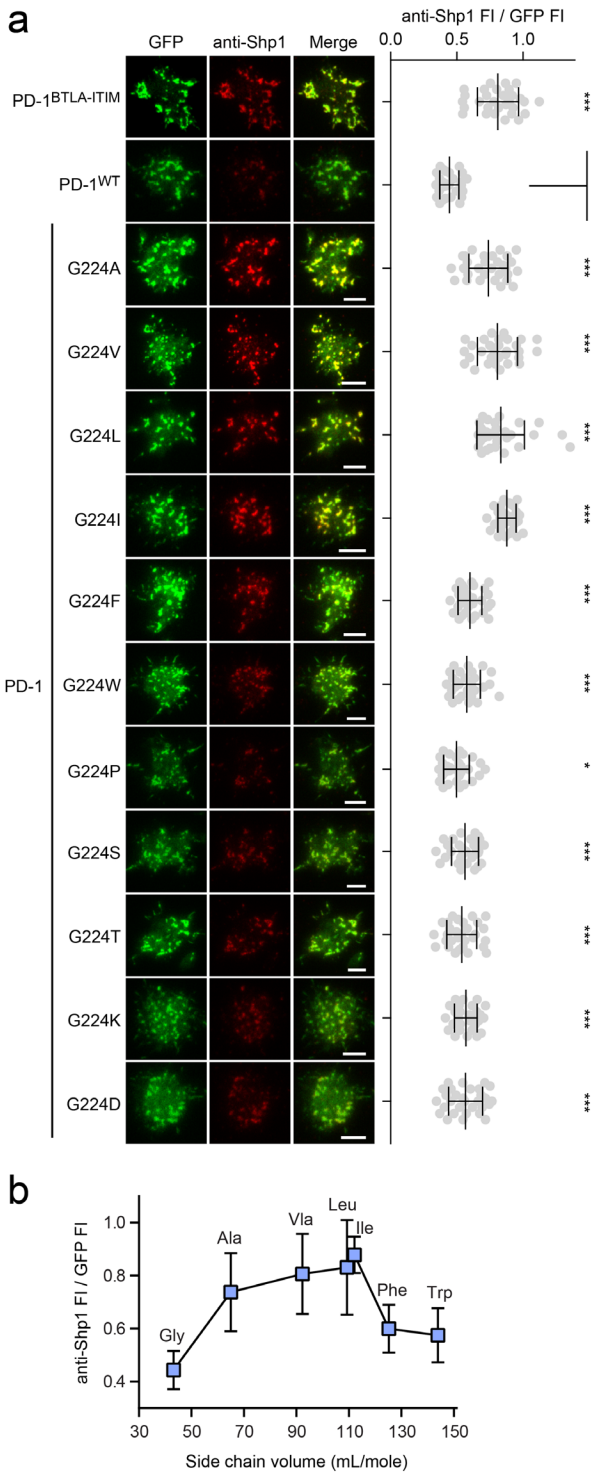

Fig. 9: A medium-sized nonpolar residue at pY+1 position of the ITIM is optimal for Shp1 recruitment.

a, Left, representative TIRF images of both PD-1 (GFP) and endogenous Shp1 (stained with anti-Shp1) in an SLB-associated Shp2 KO Jurkat cell expressing indicated PD-1 variants. Right, dot plots summarizing anti-Shp1 FI normalized to GFP FI of 30 Jurkat cells under each condition (see Methods); Error bars: s.d.. Scale bars: 5 μm. **b**, Normalized anti-Shp1 FI for a subset of PD-1 variants shown in A plotted against the nonpolar side chain volume of AA at the pY+1 position. Error bars: s.d., 30 cells. *P < 0.05; ***P < 0.001; ns, not significant; Student's t-test.

Supplementary information for

Molecular Features Underlying Shp1/Shp2 Discrimination by Immune Checkpoint Receptors

Xiaozheng Xu[1,2], Takeya Masubuchi[1,2], Yunlong Zhao[1], & Enfu Hui[1,3]*

[1]Section of Cell & Developmental Biology, Division of Biological Sciences, University of California, San Diego, La Jolla, CA 92093-0347, USA

[2]These authors contribute equally

[3]Lead Contact

*Correspondence: enfuhui@ucsd.edu

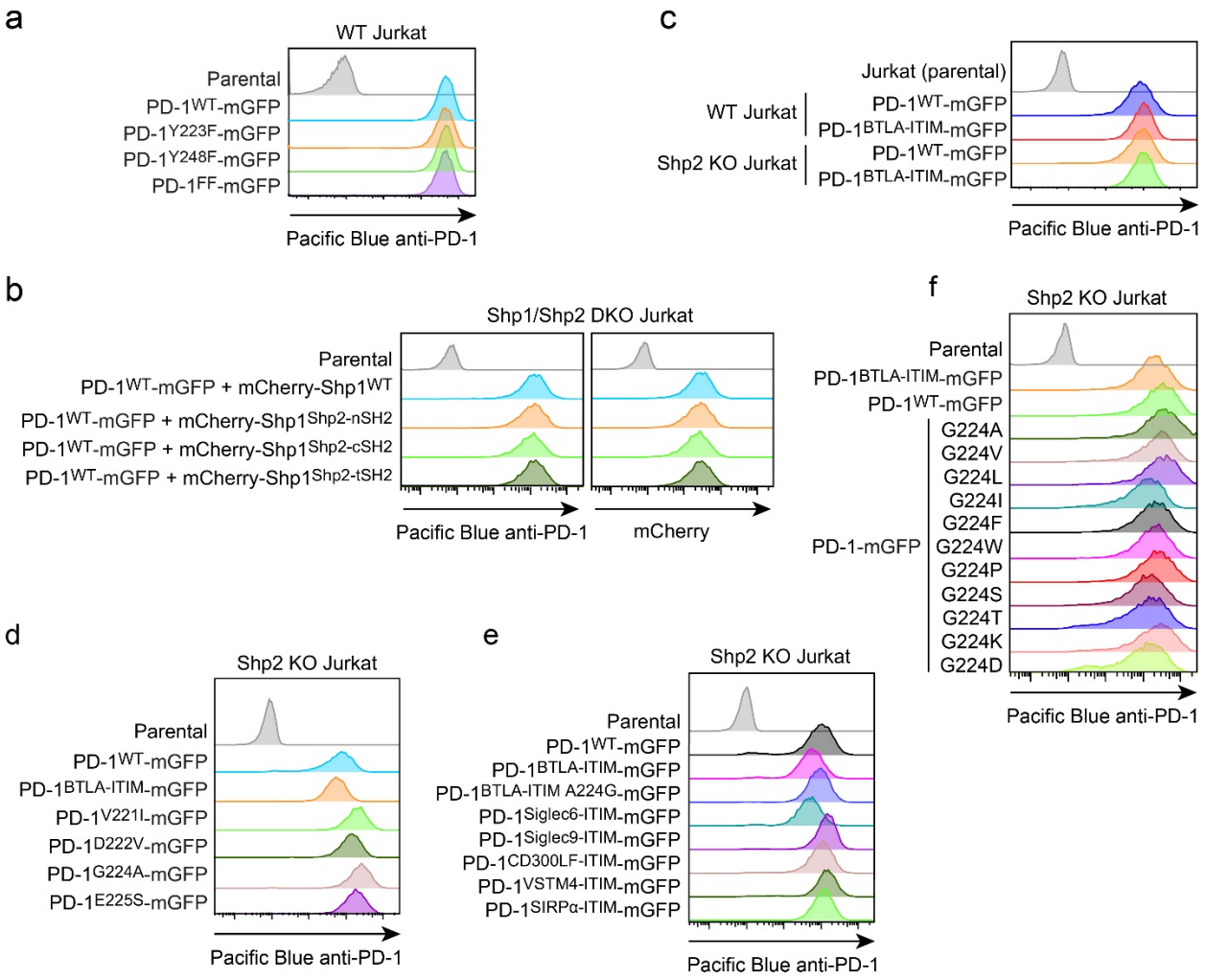

Extended Data Fig. 1 Flow cytometry histograms for Figs. 2, 4, and 7-9.

a, Flow cytometry histograms showing cell surface expressions of PD-1 variants in indicated Jurkat cells. Related to Fig. 2. **b**, Flow cytometry histograms showing cell surface expression of PD-1WT and total expressions of indicated Shp1 variants in Shp1/Shp2 DKO Jurkat cells. Related to Fig. 4. **c**, Flow cytometry histograms showing cell surface expression of indicated PD-1 variants in WT or Shp2 KO Jurkat cells. Related to Fig. 7. **d-f**, Flow cytometry histograms showing cell surface expression of indicated PD-1 variants in Shp2 KO Jurkat cells. Related to Fig. 8a-c, Fig. 8d-f and Fig. 9, respectively.

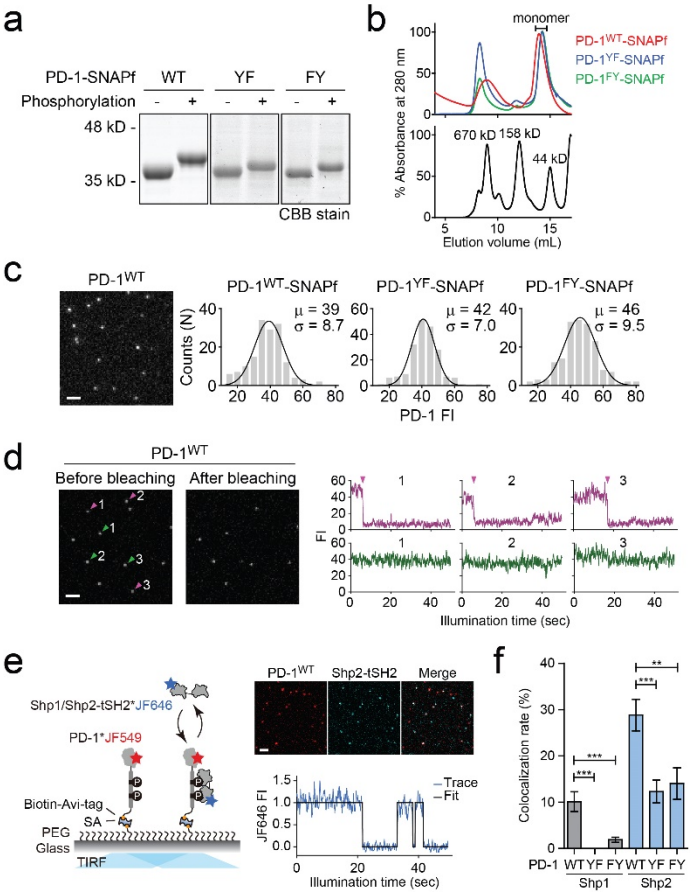

Extended Data Fig. 2 Single molecule imaging monitoring Shp1/Shp2-tSH2 binding to PD-1 variants.

a, Coomassie-stained SDS-PAGE images showing the shift of electrophoretic mobilities of indicated PD-1 variants after phosphorylation. **b**, Size exclusion chromatograms of phosphorylated PD-1 variants (top) and protein standards with their molecular weights labeled in kilo Delton (kD, bottom). The monomeric fractions used for single molecule imaging assays are indicated. **c**, Left, a representative TIRF image showing JF646-labeled PD-1 single molecules. Right, histograms summarizing the FI of individual molecules of PD-1 in the TIRF image. Mean (μ) and s.d. (σ) of the Gaussian fit are indicated distribution. Scale bar: 2 μm. **d**, Left, representative TIRF images showing JF646-labeled PD-1 single molecules before and after photobleaching. The bleached and un-bleached spots were indicated with purple and

green arrowheads, respectively. Right, fluorescence time trajectories of bleached (purple) and non-bleached (green) spots, with the bleaching moments indicated with arrow heads. Scale bar: 2 μm. **e**, Left, a cartoon depicting the setup of single molecule imaging assay. Each of the pre-phosphorylated, biotinylated, and JF549-labeled PD-1 variants was immobilized onto a biotin-PEG coated coverslip. The FIs of PD-1 molecules and the bound JF646-labeled Shp1/Shp2-tSH2 were monitored by TIRF-M. Right, representative TIRF images showing the PD-1^{WT} and Shp2-tSH2 single molecules (top), and a representative time trajectory showing Shp2-tSH2 binding and unbinding from PD-1^{WT} (bottom). Scale bar: 2 μm. **f**, Bar graphs summarizing the % of PD-1 molecules associated with Shp1-tSH2 or Shp2-tSH2 (see Methods). Error bars are s.d. from three independent experiments. **$P < 0.01$; ***$P < 0.001$; Student's t-test.

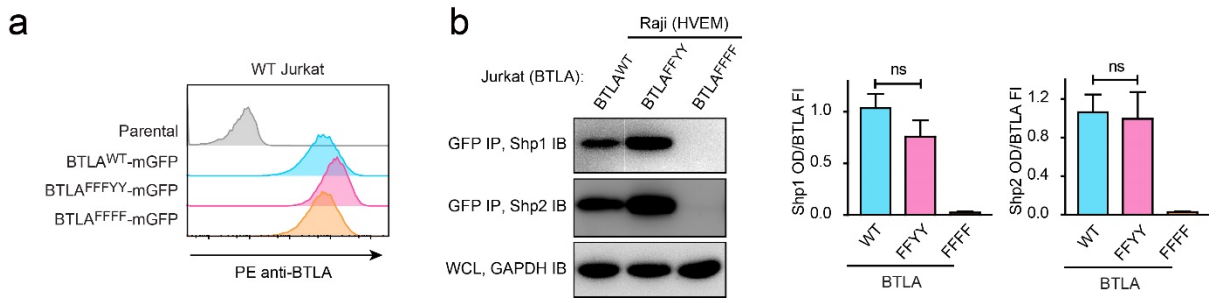

Extended Data Fig. 3. Y226 and Y243 are dispensable for Shp1/Shp2 recruitment by BTLA.

a, Flow cytometry histograms showing BTLA surface expressions in the indicated Jurkat cells. **b**, Representative IBs showing the levels of Shp1 and Shp2 bound to the mGFP-tagged BTLA variants captured by GFP IP. GAPDH IB of the WCL served as a loading control. Right, bar graphs summarizing Shp1 OD and Shp2 OD normalized to the FI of the corresponding BTLA variants, based on flow cytometry data in A. Error bars are s.d. of three independent experiments. ns, not significant in Student's t-test.

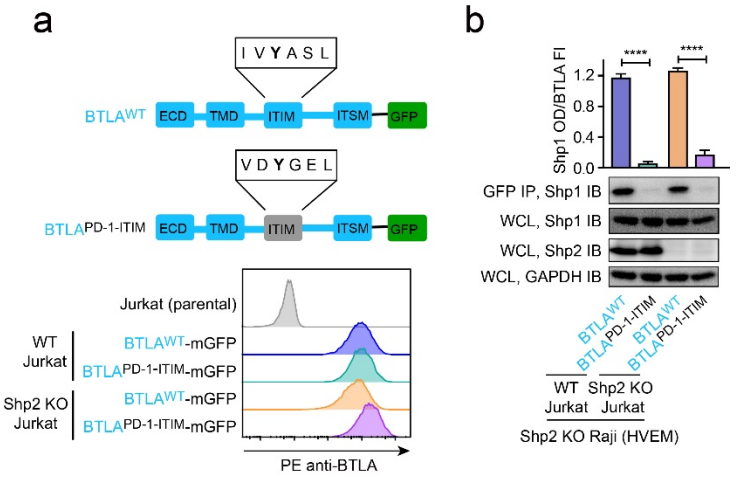

Extended Data Fig. 4 Replacing BTLA-ITIM with PD-1-ITIM abolished BTLA:Shp1 interaction in Jurkat cells.

a, Upper, cartoons depicting the domains and motifs of $BTLA^{WT}$-mGFP and $BTLA^{PD\text{-}1\ ITIM}$-mGFP. Lower, flow cytometry histograms showing the cell surface expressions of BTLA variants in the indicated Jurkat cells. **b**, Representative IBs showing the levels of Shp1 bound to mGFP-tagged BTLA variants pulled down from the indicated co-culture lysates via GFP IP. Shp1 IB and Shp2 IB of the WCL indicate their input. GAPDH IB of WCL serves as a loading control. The bar graphs on top summarizes Shp1 OD normalized to the FI of each BTLA variant, based on flow cytometry data in A. Error bars are s.d. from three independent experiments. ****$P < 0.0001$; Student's t-test.

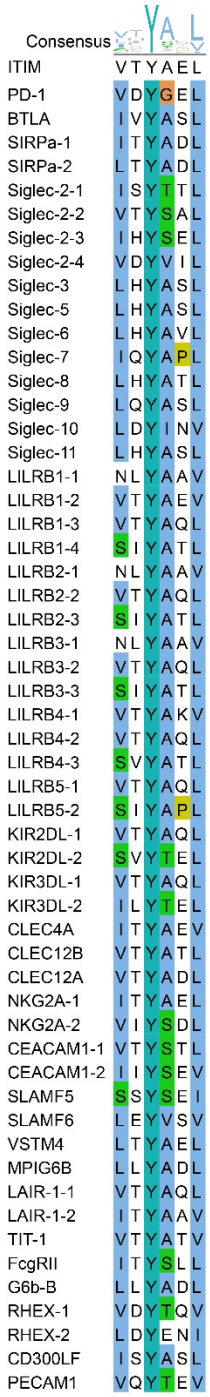

Extended Data Fig. 5 Sequence alignment of ITIMs in immune receptors.

ITIM sequences in indicated immune receptors were aligned and visualized using ClustalW and JalView. Consensus amino acids at each position in ITIM are indicated at the top.

Supplementary Table 1. K_d values of individual SH2 of Shp1/Shp2 and phosphorylated ITIM/ITSM of PD-1/BTLA; mean±s.d. (n=3).

K_d (μM)	PD-1-ITIM	PD-1-ITSM	BTLA-ITIM	BTLA-ITSM
Shp1-nSH2	0.27 ± 0.1	0.083 ± 0.020	0.064 ± 0.012	n.d.
Shp1-cSH2	n.d.	1.7 ± 1.4	1.8 ± 0.20	0.86 ± 0.31
Shp2-nSH2	0.38 ± 0.10	0.14 ± 0.049	0.34 ± 0.082	2.1 ± 1.1
Shp2-cSH2	1.4 ± 0.57	0.10 ± 0.029	1.1 ± 0.54	1.1 ± 0.19

n.d.: not detected

Supplementary Table 2. ∆G of PD-1/BTLA interactions with Shp1/Shp2-tSH2 in a parallel or an anti-parallel mode.

∆G (kJ)[a]	Parallel	Anti-Parallel
PD-1:Shp1tSH2	-70.4	-40.4
PD-1:Shp2tSH2	-76.6	-72.5
BTLA:Shp1tSH2	-75.7	-32.8
BTLA:Shp2tSH2	-70.9	-66.4

a: ∆G=RT*ln (Kd)

T=298.15 K, R is molar gas constant, R=8.314×10^{-3} kJ/K/M

Supplementary Table 3. ΔG of ITIM/ITSM and SH2 bindings.

ΔG (kJ)[a]	Shp1-nSH2	Shp1-cSH2	Shp2-nSH2	Shp2-cSH2
PD-1-ITIM	-37.5	0.0	-36.6	-33.4
PD-1-ITSM	-40.4	-32.9	-39.1	-40.0
BTLA-ITIM	-41.1	-32.8	-36.9	-34.0
BTLA-ITSM	0.0	-34.6	-32.4	-34.0

a: ΔG=RT*ln (Kd);

T=298.15 K, R is molar gas constant, $R=8.314\times10^{-3}$ kJ/K/M

Supplementary Table 4. Immune receptors harboring both ITIM and ITSM

Receptor	ITIM Y position (AA)	ITSM Y position (AA)	ITIM-ITSM distance (AA)[a]
PD-1	223	248	25
BTLA	257	282	25
Siglec-3	340	358	18
Siglec-5	520	544	24
Siglec-6	426	446	20
Siglec-9	433	456	23
Siglec-11	644	668	24
CD300LF	249	284	35
VSTM4	289	310	21
SIIRPα	429 470 496	453	24 -16 -43
SLAMF5	341	279 316	-62 -25
SLAMF6	274	285 309	11 35
PECAM1	690	713	23
MPIG6B	211	237	26

AA: amino acids

ITIM: immunoreceptor tyrosine-based inhibition motif

ITSM: immunoreceptor tyrosine-based switch motif

a: Calculated as (ITSM Y position)-(ITIM Y position)